

Vincent, S. J., Guo, L., Flecker, R., BouDagher-Fadel, M. K., Ellam, R. M. and Kandemir, R. (2018) Age constraints on intra-formational unconformities in Upper Jurassic-Lower Cretaceous carbonates in northeast Turkey; geodynamic and hydrocarbon implications. *Marine and Petroleum Geology*, 91, pp. 639-657. (doi:[10.1016/j.marpetgeo.2018.01.011](https://doi.org/10.1016/j.marpetgeo.2018.01.011))

This is the author's final accepted version.

There may be differences between this version and the published version. You are advised to consult the publisher's version if you wish to cite from it.

<http://eprints.gla.ac.uk/157982/>

Deposited on: 26 February 2018

Enlighten – Research publications by members of the University of Glasgow
<http://eprints.gla.ac.uk>

Accepted Manuscript

Age constraints on intra-formational unconformities in Upper Jurassic-Lower Cretaceous carbonates in northeast Turkey; geodynamic and hydrocarbon implications

Stephen J. Vincent, Li Guo, Rachel Flecker, Marcelle K. BouDagher-Fadel, Robert M. Ellam, Raif Kandemir

PII: S0264-8172(18)30011-4

DOI: [10.1016/j.marpetgeo.2018.01.011](https://doi.org/10.1016/j.marpetgeo.2018.01.011)

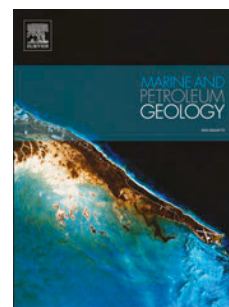
Reference: JMPG 3201

To appear in: *Marine and Petroleum Geology*

Received Date: 10 August 2017

Revised Date: 30 November 2017

Accepted Date: 10 January 2018



Please cite this article as: Vincent, S.J., Guo, L., Flecker, R., BouDagher-Fadel, M.K., Ellam, R.M., Kandemir, R., Age constraints on intra-formational unconformities in Upper Jurassic-Lower Cretaceous carbonates in northeast Turkey; geodynamic and hydrocarbon implications, *Marine and Petroleum Geology* (2018), doi: 10.1016/j.marpetgeo.2018.01.011.

This is a PDF file of an unedited manuscript that has been accepted for publication. As a service to our customers we are providing this early version of the manuscript. The manuscript will undergo copyediting, typesetting, and review of the resulting proof before it is published in its final form. Please note that during the production process errors may be discovered which could affect the content, and all legal disclaimers that apply to the journal pertain.

Age constraints on intra-formational unconformities in Upper Jurassic-Lower Cretaceous carbonates in northeast Turkey; geodynamic and hydrocarbon implications

Stephen J. Vincent^{1,*}, Li Guo¹, Rachel Flecker², Marcelle K. BouDagher-Fadel³, Robert M. Ellam⁴ & Raif Kandemir⁵

¹CASP, West Building, Madingley Rise, Madingley Road, Cambridge, CB3 0UD, UK
(stephen.vincent@casp.cam.ac.uk)

²BRIDGE, School of Geographical Sciences and Cabot Institute, University of Bristol, University Road, Bristol, BS8 1SS, UK (R.Flecker@bristol.ac.uk)

³University College London, 2 Taviton Street, London WC1H 0BT, UK (m.fadel@ucl.ac.uk)

⁴Scottish Universities Environmental Research Centre (SUERC), Scottish Enterprise Technology Park, Rankine Ave., East Kilbride, G750QF, UK (Rob.Ellam@glasgow.ac.uk)

⁵Recep Tayyip Erdoğan University, Department of Geological Engineering, 53000, Fener-Rize, Turkey
(raif.kandemir@erdogan.edu.tr)

*Corresponding author

Abstract

Upper Jurassic-lowermost Cretaceous carbonate build-ups are imaged on seismic data in the Black Sea. They form important, untested, hydrocarbon reservoirs that are the focus of active exploration. Outcrop analogues to these build-ups around the Black Sea contain a series of subaerial exposure surfaces. The hiatuses associated with a number of these subaerial exposure surfaces have been dated in a well exposed Callovian or Upper Oxfordian to Barremian shallow-water inner platform carbonate succession (the Berdiga Formation) in the Eastern Pontides using strontium isotope stratigraphy and foraminiferal biostratigraphy. They span the latest Kimmeridgian to Tithonian or Berriasian, and the Hauterivian to Barremian. Less well constrained, but broadly contemporaneous

stratigraphic gaps in multiple successions around the Black Sea provide additional insights and point to a regional driving mechanism. The timing of hiatus formation does not correspond to periods of eustatic lowstand. It does coincide, however, with Late Tithonian to Berriasian and Hauterivian to Early Aptian episodes of rifting in the Greater Caucasus Basin, located farther to the north. Thus, it is possible that subaerial exposure was caused by rift flank uplift during periods of regional extension. Uplift due to slab break off is discounted as a control because it post-dates (rather than pre-dates) locally developed Kimmeridgian magmatism. Rift-flank uplift is likely to have also affected carbonate build-ups on the intervening rift shoulders to the eastern Black Sea, the Shatskiy Ridge and the Mid Black Sea High. At outcrop, subaerial exposure is often associated with karstification and secondary porosity development. Similar processes may have occurred in the offshore helping to enhance the reservoir quality of these exploration targets.

Keywords: Black Sea, Berdiga Formation, strontium isotope stratigraphy, Pontides, reservoir potential

1 Introduction

Hydrocarbons hosted in Tethyan Upper Jurassic reef build-ups form a major resource, with their potential exemplified by the South Yolotan–Osman (Galkynysh) field in the Amu-Dar'ya Basin, Turkmenistan. This field hosts the world's second largest gas reserves estimated to be between 13.1 trillion and 21.2 trillion cubic meters of gas in place (Gaffney, Cline and Associates, 2011 audit).

Seismic reflection data in the Black Sea appear to show a number of possible carbonate build-ups along the Shatskiy Ridge, eastern Black Sea (Nikishin et al., 2015b). Regional considerations would suggest that they are of Late Jurassic-earliest Cretaceous age. The build-ups are up to 1-2 km thick, 75 km long and 25 km wide (Afanasenkov et al., 2005, 2007). They are deeply buried (~2.5-7 km;

Meisner et al., 2009), at water depths typically greater than 2 km and are the focus of on-going exploration activity. Until they are penetrated by boreholes and the results released, we are reliant on outcrop data from Upper Jurassic-lowermost Cretaceous carbonate rocks around the margins of the Black Sea to provide insights into the nature of these offshore exploration targets.

We have carried out extensive work on these outcrop analogues (e.g. Guo et al., 2011). Observed porosities are typically less than 5%. However, at a number of key outcrops in the Pontides (Turkey), the western Greater Caucasus (Russia) and Crimea (disputed), erosive surfaces that display evidence for subaerial exposure have been observed (e.g. Figure 4 of Guo et al., 2011). Some of these are associated with karstification and secondary porosity development. This may have enhanced the reservoir characteristics of these carbonate units in the subsurface and have formed intraformational markers that can be identified on seismic sections.

Insufficient age diagnostic fauna are present within the shallow-marine carbonate outcrop analogues to determine accurately the age of these subaerial exposure surfaces. As a result, it is unclear whether they are synchronous. This uncertainty impacts upon our ability to predict their presence in the subsurface of the Black Sea basin.

This study is the first step towards addressing the paucity of age control and utilises strontium isotope stratigraphy combined with foraminiferal biostratigraphy. These techniques have been used to constrain the age of a relatively well-exposed Upper Jurassic-Lower Cretaceous carbonate-dominated platform-interior succession (locality PT09_21) in the Eastern Pontides, Turkey, which contains a number of surfaces that display evidence for subaerial exposure and / or erosion.

2 Geological background

Upper Jurassic to Lower Cretaceous strata at locality PT09_21 crop out between the villages of Kale and Nazlıçayır in the region of Gümüşhane, NE Turkey, in the Eastern Pontides. Geologically, the

region forms part of eastern Sakarya Zone, which is bounded by the Black Sea to the north and the İzmir-Ankara-Erzincan and Sevan-Akera sutures to the south (Figure 1). These sutures represent the former position of the northern Neotethys Ocean that closed due to northerly-directed subduction during Late Cretaceous to Eocene time (Okay and Şahintürk, 1997; Robertson et al., 2014; Robertson and Dixon, 1984; Şengör and Yılmaz, 1981). Closure resulted in the development of a series of mostly south-dipping, north-vergent thrust sheets in the south, whilst a more autochthonous region is preserved to the north.

The basement of the eastern Sakarya Zone comprises a pre-Upper Carboniferous high-grade metamorphic complex (the Pülür Massif) intruded by Carboniferous-Permian granitoids (Okay, 1996; Okay and Şahintürk, 1997; Topuz et al., 2004a; Topuz et al., 2004b; Topuz et al., 2007; Topuz et al., 2010). In the eastern Sakarya Zone, these are locally overlain by a thick Upper Carboniferous-Lower Permian shallow-marine to non-marine sedimentary sequence (Okay and Leven, 1996). Lastly, Permo-Triassic metabasite-marble-phyllite units are exposed in the Ağvanis and Tokat massifs (Okay and Şahintürk, 1997). Together these rocks are generally considered to represent the products of their Variscan accretion to Laurasia and the subsequent northward subduction of Paleotethys beneath this margin (Kazmin, 2006; Okay and Şahintürk, 1997; Okay and Topuz, 2017; Robinson et al., 1995).

Lower to Middle Jurassic strata unconformably overlie older rocks. They were deposited in an extensional setting and are up to 2240 m thick. In the study region they are known as the Şenköy Formation (Kandemir, 2004). Broadly speaking they form a transgressive-regressive succession comprised of basal alluvial conglomerates and sandstones, shallow-marine sandstones and possibly *Ammonitico Rosso* condensed carbonates, volcanic and volcanoclastic gravity flow deposits (that make up the majority of the succession) and, in places, an upper interval of coal- and gypsum-bearing siliciclastic rocks (Görür et al., 1983; Kandemir, 2004; Kandemir and Yılmaz, 2009; Koçyiğit and Altın, 2002; Okay and Şahintürk, 1997; Yılmaz, 2002). Facies typically become finer grained

and deeper marine towards the south (Okay and Şahintürk, 1997). Extension is attributed to roll-back during either the southerly subduction of Paleotethys to the north of the Sakarya continent (Dokuz et al., 2017; Dokuz et al., 2010; Görür et al., 1983; Koçyiğit and Altiner, 2002; Şengör and Yılmaz, 1981; Tüysüz, 1990; Yılmaz et al., 1997) or the northerly subduction of Neotethys to its south (Kaz'min and Tikhonova, 2006; Okay et al., 2014; Ustaömer and Robertson, 2010).

Relative tectonic quiescence (Okay and Nikishin, 2015), combined with a eustatic sea-level rise and climatic amelioration (Kiessling et al., 1999; Leinfelder et al., 2002), resulted in a switch to carbonate-dominated sedimentation in the eastern Sakarya Zone during Late Jurassic (or possibly latest Middle Jurassic) to Early Cretaceous time. This is reflected in the deposition of the up to 1000 m thick Berdiga Formation (Pelin, 1977) or Berdiga Limestone (Kırmacı et al., 1996). In the northern, autochthonous region, this unit formed a south-facing carbonate platform that is the focus of this study. Deeper-water sediments were deposited in what was to become the allochthonous zone to the south.

Volcanic and volcanoclastic intercalations are present in the Upper Jurassic-lowermost Cretaceous successions of the western Sakarya Zone (Altiner et al., 1991), the eastern Sakarya Zone (Dokuz et al., 2017; Konak et al., 2009; Ustaömer and Robertson, 2010) and the northern Transcaucasus (Adamia et al., 1992; Kazmin et al., 1986). The lavas in the eastern Sakarya Zone were probably generated in a within-plate setting (Dokuz et al., 2017; Ustaömer and Robertson, 2010).

3 Previous work on the Berdiga Formation

The Berdiga Formation has been studied by numerous authors (e.g. Kırmacı, 1992; Kırmacı et al., 1996; Koch et al., 2008; Koçyiğit and Altiner, 2002; Taslı et al., 1999; Yılmaz, 1992). The age of the unit, however, remains poorly constrained, in large part due to a paucity of biostratigraphic marker species. In the autochthonous northern region, for instance, authors have variously suggested that

sedimentation commenced in the Aalenian-Bajocian (Pelin, 1977), Callovian (Kırmacı, 1992; Robinson et al., 1995), Oxfordian (Koch et al., 2008) or Kimmeridgian (Dokuz and Tanyolu, 2006; Taslı et al., 1999). Callovian-aged detrital zircons in the underlying Şenköy Formation (Akdoğan et al., submitted) close to the Berdiga Formation type section near Alucra, more precisely constrain a Callovian or younger depositional onset age for the formation in this region.

Rifting disrupted sedimentation on the Berdiga carbonate platform during Cretaceous time (Eren and Taslı, 2002; Konak et al., 2009; Taslı et al., 1999; Yılmaz, 2002; Yılmaz and Kandemir, 2006). This resulted in erosion, karstification or hardground formation on the highs, and a deepening and change in carbonate facies in subsiding regions. On the highs, sedimentation typically continued until the Late Barremian (Pelin, 1977) or Early Aptian (Eren and Taslı, 2002). In the lows, deeper water carbonate-dominated sedimentation may have continued until the Turonian (Eren and Taslı, 2002; Taslı et al., 1999; Taslı and Özsayar, 1997).

A number of studies of the Berdiga Formation have been carried out in the vicinity of locality PT09_21 (Eren and Taslı, 2002; Kara-Gülbay et al., 2012; Kırmacı et al., 1996; Koch et al., 2008). Here the formation is estimated to be up to 590 m thick (Eren, 1983). The majority of these studies focussed on the upper part of the formation and a possibly lacustrine, bituminous interval or its contact with overlying units. Only the study by Koch et al. (2008) documented the lower ~320 m of the formation (although not its basal contact). They subdivided the formation into 15 units and described the facies and diagenesis of the succession in great detail in outcrops which they termed the Kırcaova section.

We revisited the Kırcaova section (our locality PT09_21E; Figure 2). The main aims of our study were to document the presence of a major erosional disconformity within the lower part of the section not recognised by Koch *et al.* (2008), constrain better the age of the section based on additional biostratigraphic and strontium isotopic determinations, and highlight the potential regional significance of this (and younger) disconformity surfaces. Our study was not designed to replicate

the facies and diagenetic aspects of Koch et al. (2008), although we have complemented it with some additional field and microscopic observations. The nature of the succession is described below and summarised in Table 1.

4 Stratigraphy and facies

The Kircaova section runs between 40.34506°N, 39.72918°E and 40.34837°N, 39.73112°E (locality PT09_21E) (Figure 1). The base of the Berdiga Formation is not exposed in this section but was observed at locality PT09_21A (40.38020°N, 39.67691°E) (Figure 3). Here, presumed Middle Jurassic volcanoclastic sediments of the Şenköy Formation are unconformably overlain by a pebbly limestone containing volcanoclastic and granitic clasts, followed by medium-bedded arenaceous limestones and thin-bedded sandstones and silty mudstones. These lithologies are poorly exposed and approximately 6 m thick.

Koch et al. (2008) subdivided the lowermost part of the Berdiga Formation into 3 units beneath a prominent lava flow (unit IV; Table 1; Figure 4) that forms a regional marker (Figure 2 and Figure 3). We augmented observations in this part of the Kircaova section with those at locality PT09_21B (40.36089°N, 39.68825°E to 40.35525°N, 39.69027°E) along a tributary of the Keçi River (Figure 3). The thickness of units I-III are taken from Koch et al. (2008). Sample positions are located on Figure 4.

Unit I is 18 m thick and consists mainly of very thick-bedded intraclastic packstones-grainstones (sample 21B_09) and intraclastic-bioclastic grainstones (sample 21B_08) deposited on a shallow-water, moderate- to high-energy platform interior (Table 1). Coated grains (oncoids) are abundant in the lower part of the unit. Benthic foraminifera (both large and small), gastropods, bivalves and corals have been recognised; locally *Tubiphytes* fragments are present. High faunal diversity was also documented by Koch et al. (2008).

Unit II is 29 m thick and is dominated by medium- to thick-bedded dolostones (samples 21B_07 and 21B_06). The original textures of many dolostones are obscured. Some dolostones show ghost textures of grainstones with bioclasts, lithoclasts and ooids, as well as matrix-rich peloidal and lithoclastic packstones that lack bioclasts (Koch et al., 2008). Koch et al. (2008) suggested that this unit was mainly deposited in a restricted platform interior during decreased energy levels, interrupted by episodes of open and higher energy conditions.

Unit III is 23 m thick and comprises mainly medium- to thick-bedded dolostones in the lower part (sample 21B_05) and lime mudstones in the upper part (sample 21E_01) (Table 1). They contain traces of benthic foraminifera and other bioclasts and were continuously formed in a restricted shallow-marine platform interior (Koch et al., 2008). Traces of volcanic rock fragments indicate the presence of contemporaneous volcanic activity (Koch et al., 2008). A gastropod floatstone with meteoric dissolution and cementation features occurs near the top of the unit at locality PT09_21E (sample 21E_02; Figure 5A).

Unit IV is 10 m thick and dominated by a highly weathered doleritic lava flow with plagioclase phenocrysts and calcite amygdales (samples 21B_01 and 21E_03) (Table 1; Figure 4). Pillow structures, entrained rafts of contorted limestone (sample 21B_04) and breccia lenses suggest subaqueous eruption. Our Ar-Ar dating of plagioclase crystals from this unit yielded an erroneously young (Aptian) age, most likely due to argon loss because of the altered nature of the material. The top of the unit is capped by greenish tuffaceous siltstones and reddish silty mudstones that were likely deposited in near shore or subaerial environments. This unit has previously been referred to as the Olivine dolerite sill (Tokel, 1972), Diabase member (Eren, 1983), Keçidere basalt (Taslı, 1997), Diabase sill (Koch et al., 2008) or part of the Kuşakkaya Member (Dokuz et al., 2017).

Unit V is up to 54 m thick and comprises a cliff-forming interval of thick-bedded lime mudstones (samples 21B_02, 21B_03, 21E_10, 21E_11 and 21E_12) (Figure 2, Figure 5B and Figure 6A-B). It likely represents deposition in a low energy, restricted shallow-water environment. Altered volcanic

rock fragments have also been documented (Koch et al., 2008). The top of unit V is marked by a pronounced erosion surface with up to 45 m of local relief (Figure 2, Figure 4 and Figure 6A-B). Along the edge of this incised valley, the underlying limestones are brecciated (Figure 6C) and cut by fissures and cracks that are filled with brownish and greenish clays. It is likely that the erosion surface was formed during subaerial exposure. Koch et al. (2008) did not identify this surface.

Above the disconformity surface, the subdivisions of Koch et al. (2008) are less distinctive. Unit VI is up to ~62 m thick. Initial, incised valley filling sediments consist mainly of the following: limestone breccias; fine-grained conglomerates; scoured, laminated, cross-laminated and cross-bedded sandstones; lime mudstones; and dolostones with laminated structures (e.g. samples 21E_04 to 21E_06) (Figure 4). Abundant quartz, angular limestone and volcanic clasts are present. Sandstone sample 21E_04 is a volcanic lithic arkose, presumably reflecting the nearby erosion of unit IV or its equivalents. The upper part of unit VI on the shoulder of the incised valley comprises poorly exposed, medium- to thick-bedded dolostones (samples 21E_07 and 21E_08) (Figure 2, Figure 4 and Figure 6A-B). This part of the unit was also recorded by Koch et al. (2008) who documented lime mudstones with traces of ostracods, which could represent deposition in a low energy, restricted shallow-water environment.

Unit VII is 57 m thick and poorly exposed. The base of the unit is marked by dolostones with abundant quartz granules. Upward, further dolostones are exposed (samples 21E_13 and 21E_14; Figure 5C); some contain ghost textures of peloids and intraclasts (sample 21E_09). Ghost textures of molluscs and echinoids have been described by Koch et al. (2008) who suggested that this unit was formed in a more open shallow-marine environment with high energy conditions.

Unit VIII is 5 m thick and comprises well exposed medium- to thick-bedded intraclastic and bioclastic, coated grain packstones and grainstones with abundant foraminifera (samples 21E_15 to 21E_17) (Figure 2 and Figure 5D). This unit represents deposition in a high energy, open shallow-water environment.

Unit IX is 30 m thick and is dominated by well exposed medium- to thick-bedded, dolomitised bioclastic wackestones (samples 21E_18 to 21E_20) (Figure 4). These were probably deposited in low to moderate water energy conditions.

Units X-XII are ~57 m thick and only poorly to moderately exposed (Figure 2 and Figure 4). They comprise medium- to thick-bedded intraclastic and bioclastic wackestones, packstones and grainstones (e.g. Figure 5E) that have undergone differing amounts of dolomitisation (samples 21E_21 to 21E_23).

The top of the logged succession forms prominent cliffs (Figure 2). Units XIII-XIV are ~24 m thick and are characterised by three prominent erosion surfaces (B-D) that are each overlain by reddened breccio-conglomerates composed predominantly of limestone clasts (Figure 4 and Figure 6D-G). Erosion surface C separates limestones cut by fissures filled with clays, below, from carbonate clasts that are cemented in a meniscus style above (Figure 5F). Koch et al. (2008) also mentioned mud cracks and soils associated with these erosion surfaces. The remainder of the interval comprises a wide variety of lithologies including sandstone, foraminifera packstone-grainstone, mollusc floatstone, intraclastic and bioclastic grainstone, bioclastic wackestone, lime mudstones and laminated stromatolites (e.g. samples 21E_24 to 21E_30) indicative of varying energy, shallow-water conditions. Koch et al. (2008) reported an increased presence of volcanic rock fragments and quartz grains.

Unit XV is at least 19 m thick and comprises thick-bedded bioclastic packstones and grainstones with minor lime mudstone interbeds (samples 21E_31 to 21E_33). Algal laminations and large bivalves are evident and Koch et al. (2008) recorded local birdseye structures suggesting a shallow, possibly intertidal, environment.

We did not record data from Koch et al. (2008)'s final unit XVI. According to these authors it is 23 m thick and comprises interbeds of intraclastic, foraminiferal wackestones, packstones and grainstones.

5 Diagenesis

The main diagenetic processes in the Berdiga Formation are micritisation, cementation, karstification, dissolution, compaction and dolomitisation. Micritisation resulted in the formation of micritic envelopes around original grains and is common in intraclastic bioclastic grainstones in the Kircaova section (Figure 5A). Cementation resulted in different generations of cements that are irregularly developed. Early formed isopachous cements line cavities in intraclastic-oid and intraclastic-bioclastic grainstones (Figure 5D). Drusy mosaic (Figure 5D), blocky spar and poikilotopic cements commonly fill the remaining pore space. Pendant and meniscus cements are typically formed due to gravitation in meteoric-vadose environments (Figure 5A, F). Karstification was observed beneath the lava flow and erosion surfaces A to C. Dissolution vugs filled with blocky calcite cements occur locally. Intense dolomitisation is pervasively developed throughout much of the succession. Dolomites contain early formed fine-grained subhedral dolomite crystals (Figure 5C) and, in places, coarse-grained, late replacive, rhombohedra (Figure 5B). Additional diagenetic details can be found in Koch et al. (2008).

6 Age control

6.1 Microfauna

No age diagnostic macrofauna were observed in the field. Instead multiple thin sections were made for each of the samples and these were examined using a transmitted light petrological-type

microscope in order that their micropaleontological components could be identified. The results are presented as Table 2, with key forms illustrated in Figure 7. The age of diagnostic assemblages, based on BouDagher-Fadel (2008, 2012, 2015), are consistent with their stratigraphic position and range from Bathonian-Oxfordian to Late Barremian-Aptian (Figure 4).

6.2 Strontium isotope stratigraphy

6.2.1 Sampling strategy

The Sr isotope ratio of ocean water has varied throughout earth history and has been calibrated to provide a powerful chronostratigraphic tool (e.g. McArthur et al., 2001). The method relies on biogenic carbonate preserving the $^{87}\text{Sr}/^{86}\text{Sr}$ of marine water (Burke et al., 1982; Elderfield, 1986). Secondary alteration can however result in Sr isotope ratios that reflect either freshwater run-off or pore water chemistry. Consequently, it is important to target and analyse only carbonate where there is no evidence of post-depositional diagenesis. Some studies advocate trace element geochemistry to identify samples that have enhanced concentration of e.g. Fe and Mn through diagenetic alteration that can be excluded from strontium isotope stratigraphy (e.g. Denison et al., 1994; Kuznetsov et al., 2012). While trace element composition undoubtedly has a role in identifying diagenetic alteration, especially when attempting to reconstruct seawater $^{87}\text{Sr}/^{86}\text{Sr}$ using whole-rock limestones (e.g. Denison et al., 1994), it is unclear whether these specific criteria are robust for samples of differing geological age and/or sedimentary environment. In this study we prefer to assess diagenesis by petrographic examination and exclude altered material by careful micro-sampling.

Samples were thin sectioned, stained for calcite and dolomite and inspected under a polarising microscope. Carbonate shells with well-preserved micro-structure and areas of biogenic lime mud were identified on the thin section and then highlighted on the rock chip from which the thin section

had been made. A micro-drill was used to generate carbonate powder from the highlighted area with a typical sample spot size of ~2 mm. Every attempt was made to avoid material likely to have undergone diagenetic alteration, for instance aragonitic or high-Mg calcite shells with poor microstructure preservation, dolomite or carbonate veins. In some instances, however, it was not possible to be sure that only primary biogenic carbonate was sampled as drilling occurs out of the plane of the thin section.

Samples were leached in 1N ammonium acetate (Gorokhov et al., 1995) and then dissolved in 2.5 M HCl. Residual Sr/silicate impurities were rejected by centrifugation. Sr was separated using SrSpec[®] resin (Eichrom Technologies LLC). Samples were loaded onto Re filaments with a Ta₂O₅ activator and measured on a VG Sector 54-30 mass spectrometer in dynamic multi-collection mode. Mass fractionation was corrected using the exponential law and $^{86}\text{Sr}/^{88}\text{Sr} = 0.1194$. During the course of this study NIST SRM987 gave $^{87}\text{Sr}/^{86}\text{Sr} = 0.710260 \pm 0.000018$ (2σ) which is within error of the consensus SRM987 value (0.710248) suggested by McArthur et al. (2001). To be entirely consistent with this consensus value our data could be adjusted by (0.710248/0.710260) but we have not applied such a correction because we do not seek to misrepresent the uncertainty inherent in the Sr isotope method.

6.2.2 Results

Nineteen samples were analysed for their Sr isotope ratio (Table 3). When compared with the Sr isotope seawater curve (McArthur et al., 2012), these values correspond to multiple possible ages because the curve varies considerably through this period of the Mesozoic (Figure 8, insert). However, biostratigraphic information from the section (Table 2) provides constraints on which of these ages are mostly likely to correspond to the Sr isotope ratio measured. In addition, stratigraphic integrity must be maintained and this also excludes some possible age interpretations of the

$^{87}\text{Sr}/^{86}\text{Sr}$ values (Table 3). Of the nineteen samples analysed, sixteen provide ages that are compatible with both these constraints and indicate a stratigraphic section spanning the Callovian or Oxfordian to Barremian, a period of c. 35 Ma (Figure 4). This suggests that the Sr isotope ratios measured reflect the primary Sr isotope ratio of coeval seawater and consequently provide robust age constraints on the section. Absolute age values are taken from Gradstein et al. (2012).

Samples 21B_08, 21E_02, 21B_03, 21E_05, 21E_06, 21E_14, 21E_17 and 21E_23 are relatively straightforward to interpret because they are consistent with the biostratigraphic information and preserve stratigraphic integrity (Table 3). Nine samples are slightly more complicated to interpret and are discussed below.

Samples HUR8 and 21B_09 were collected stratigraphically ~4 m apart. Their Sr isotope ratios are within analytical error of each other and lie close to a minima on the Sr isotope seawater curve, such that two age ranges are possible; 166-164 Ma (Early to Middle Callovian) and 160-155 Ma (Middle Oxfordian to Early Kimmeridgian) (Table 3 & Figure 4). Foraminiferal constraints from samples within this part of the section suggest that it is no younger than Oxfordian in age.

Sample 21E_11 has a slightly higher Sr isotope ratio than overlying sample 21E_12. This is also the case for sample 21E_27 relative to overlying sample 21E_29. Given the increasing Sr isotopic ratio values with decreasing age on the Kimmeridgian to Hauterivian limb of the Sr isotope seawater curve (Figure 8), these samples appear to be in the wrong stratigraphic order. However, the Sr isotopic values of both pairs of samples are within analytical error, such that ages common to both are permissible and further restrict their likely age ranges (Figure 4).

Two analyses were taken from sample 21E_30, one from a rudist shell and another from the micritic infill of that shell. Both samples are within error of each other, but yielded strontium ratios that are higher than the best estimate of oceanic values in the Early Cretaceous (Figure 8). The $^{87}\text{Sr}/^{86}\text{Sr}$ for the rudist lies within the Sr isotope seawater curve uncertainty, while only the analytical error for

the micritic sample overlaps with the top of the uncertainty on the Sr isotope seawater curve. The age of this sample is therefore estimated as being at the highest point of the Early Cretaceous strontium curve (Figure 8), but its exact age should be treated with caution.

Sample PT09_SV_021E_32 was sampled close to a carbonate vein (Table 3), but in this instance the Sr ratio measured corresponds with an age compatible with biostratigraphic constraints and relative stratigraphic position. However, the age of this sample should be treated with caution.

Three samples, HUR9, 21B_08 and 21E_028, yielded Sr isotope ratios incompatible with their stratigraphic relationship to other dated samples and with foraminiferal biostratigraphic constraints. In the case of 21B_08, this is likely to be the result of including some diagenetic Sr from an adjacent carbonate vein (Table 3). Although we attempted to sample dense micritic elements within samples HUR9 and 21E_28, it is also possible that they included some diagenetic Sr from diffuse dissolution voids.

6.3 Discussion

The top of the Berdiga Formation was not sampled in this study and therefore the age of the formation range cannot be constrained. However, our Sr and biostratigraphic analysis indicates that it must span from at least c. 158 Ma to c. 127 Ma (Late Oxfordian - Late Barremian; Figure 4 and Figure 9a) at this locality. The base of the section could be Callovian in age.

Within the lower part of the succession, there appears to be an increase in carbonate sedimentation rate from between ~5-41 m/Ma in units I-III to above 43 m/Ma in unit V above the lava flow (Figure 4). The lava flow itself is probably Late Kimmeridgian in age. This is younger than the estimates of Taslı (1997) (Late Oxfordian-Early Kimmeridgian) and Koch et al. (2008) (Middle Kimmeridgian). Dokuz et al. (2017) dated the lava flow to between 155-150 Ma (Late Kimmeridgian-Early Tithonian) based on the fossil data of Koch et al. (2008); it is unclear whether the difference in

reported age between these sources results from the reinterpretation of species ranges or simply the use of a chronostratigraphic scheme other than Gradstein et al. (2012).

The age range of missing strata at the pronounced disconformity at the top of unit V (Figure 2), as constrained by samples 21E_11 and 21E_12, and sample 21E_05, spans 9-13 million years from the very latest Kimmeridgian to somewhere in the Berriasian (Figure 4 and Figure 9a). However, because sample 21E_05 was not collected from the base of the incised valley fill, the age gap will have been shorter. Extrapolation of sedimentation rates suggests that sedimentation could have resumed by the latest Tithonian.

Sedimentation rates in units VI-XII above the lower disconformity surface (A) have increased with time from between ~5-18 m/Ma to above 102 m/Ma (Figure 4). This is likely to reflect intermittent high-energy conditions and sediment bypassing within the incised valley, followed by more continuous sedimentation and carbonate production during the re-establishment of the carbonate platform in overlying units.

The 3 hiatuses and intervening sediments within units XIII-XIV occur within an interval spanning between 3-6 million years during the Hauterivian to Barremian (Figure 4 and Figure 9a). Sedimentation rates in the upper part of unit XIV and XV appear to have been relatively slow. This is similar to the situation above erosion surface A and is probably a result of bypass / intermittent erosion as reflected in the relatively coarse-grained, high-energy nature of these sediments.

7 Insights from other Black Sea outcrops

Insights into the significance of, and controls on, hiatus formation in the Eastern Pontides, can be gained by reviewing the location and age of other Upper Jurassic to Lower Cretaceous successions in the Black Sea region (Figure 9).

In the Central Pontides, we examined a section south of Küre at locality PT09_017 (41.70450°N, 33.69394°E; Figure 1 and Figure 9b). Its basement comprises Upper Triassic phyllites intruded by the Ağlı Porphyry that yielded a 154 ± 2 Ma Rb-Sr cooling age (Aydın et al., 1995). This constrains the maximum depositional age of overlying basal conglomerates (locally known as the Bürnük Formation) that pass gradationally up into up to ~80 m of shallow-water carbonates of the İnaltı Formation. The İnaltı and Berdiga formations are roughly age equivalent (Figure 9). The carbonates are overlain by conglomerates of the Çağlayan Formation via a disconformity that has a local incisional relief of ~50 m. Similar stratigraphic patterns have been observed elsewhere in the Central Pontides (Derman and İztan, 1997; Kaya and Altıner, 2015; Okay et al., 2017) (Figure 9c). Our biostratigraphic determinations from locality PT09_017 indicate a Kimmeridgian-Tithonian age range for the carbonate succession (Table 4). In addition, a single strontium isotope ratio measured from 5 m below the top of the İnaltı Formation (sample 17_15) yields a value (0.707211 ± 0.000026) that equates to an Early Berriasian age (145.05-142.05 Ma) and constrains the minimum age of carbonate deposition (Figure 9b). This is consistent with the Kimmeridgian to Early Berriasian biostratigraphic ages for the İnaltı Formation obtained from similar outcrops in the Central Pontides by Okay et al. (2017) (Figure 9c). Analysis of a microbial overgrowth in the overlying conglomeratic Çağlayan Formation yielded a strontium isotope value (0.708037 ± 0.000036) incompatible with the age of the underlying sediments. The work of Okay et al. (2017) would suggest that the Çağlayan Formation is probably mid Barremian or younger in age (Figure 9c) and therefore equivalent to sediments deposited above erosion surface D at Kırcaova (Figure 9a).

Observations from the Central Pontides highlight two things. Firstly, carbonate deposition continued through the Tithonian and into the Early Berriasian (Figure 9b, c). If the same were true for the Eastern Pontides, this would suggest that much of the hiatus associated with erosion surface A at Kırcaova resulted from the post-depositional erosion of uppermost Kimmeridgian to Lower Berriasian strata rather than from non-deposition. Secondly, sediments equivalent to those deposited between erosion surfaces A and D at Kırcaova have not yet been recognised (Figure 9).

Either (i) the Central Pontides was a region of uplift and non-deposition during this time period (Okay et al., 2017), (ii) sediments were removed by later relative base-level falls equivalent to those responsible for erosion surfaces B-D at Kırcaova or (iii) sediments, potentially similar to the İncigez Formation developed farther west (see below; Figure 9d), are present but have yet to be recognised.

In the İstanbul Zone of the Western Pontides, we examined a section around Zonguldak at locality PT09_003 (41.42279°N, 31.73215°E; Figure 1 and Figure 9d). As in the Central Pontides, carbonate-dominated sediments overlie a conglomerate-draped unconformity. These carbonates were originally also named the İnaltı Formation and mapped to be Late Jurassic to Early Cretaceous in age (Ketin and Gümüş, 1963). Subsequent mapping, however, identified an important disconformity separating Kimmeridgian to Berriasian carbonates from undated overlying continental red beds that fill an irregular topography (Derman and İztan, 1997; Derman and Sayılı, 1995). These are overlain by further carbonates of Late Barremian-earliest Aptian age (Masse et al., 2009). Based on these observations, the İnaltı Formation was redefined to form only the lower part of this carbonate sequence (Derman and İztan, 1997; Derman and Sayılı, 1995). The red beds were named the İncigez Formation and the upper carbonate sequence, the Öküşmedere Formation (Figure 9d).

Observations from the Western Pontides highlight four things. Firstly, the major disconformity developed here may have been triggered by the same relative base-level fall responsible for erosion surface A at Kırcaova. Secondly, the barren İncigez Formation represents sedimentation between erosion surfaces A and D. Derman and İztan (1997, their figure 2) originally placed this formation in the uppermost Valanginian to Hauterivian (Figure 9d). However, if the same sedimentary responses are common across the Pontides, our work would suggest that this unit is likely to be equivalent to the Berriasian to Valanginian incised valley fill of unit VI at Kırcaova (Figure 4 and Figure 9a). Thirdly, the Upper Barremian to lowermost Aptian Öküşmedere Formation, like the Çağlayan Formation, represents sediment time equivalent to those deposited above erosion surface D at Kırcaova (Figure 9d). Fourthly, if the disconformity surfaces observed at Kırcaova can be documented to be of

mappable extent then, just as has happened in the Western Pontides, it would be good stratigraphic practise to rename the individual components here to reflect their genetic disconnection, with the Berdiga Formation term being restricted to Jurassic strata only.

Given that most tectonic models propose that Black Sea oceanic spreading occurred sometime in the Cretaceous to Eocene (e.g. Görür, 1988; Kazmin et al., 2000; Nikishin et al., 2015a; Okay et al., 2013), the Caucasus and Crimea would have been broadly contiguous with the Eastern Pontides during Late Jurassic-Early Cretaceous carbonate deposition. Observations from these regions are therefore also considered below.

The only strontium isotope stratigraphy studies published on similarly-aged carbonate platform sediments in the Black Sea region are from the Baydar region of southwest Crimea (Rud'ko et al., 2017) and the Demerdzhi Plateau in central Crimea (Rud'ko et al., 2014). Both of these studies yielded 6 reliable $^{87}\text{Sr}/^{86}\text{Sr}$ values from carbonate platform facies of the Yalta Formation and imply c. 153.7-151.8 Ma and c. 153.1-148.8 Ma (Late Kimmeridgian to Early Tithonian) age ranges, respectively (Figure 9e, g). As in the Central and Western Pontides, this indicates that carbonate deposition was on-going during the period represented by hiatus A at Kırcaova.

Rud'ko et al. (2017) also dated part of the overlying Baydar Formation in the Baydar region to be Early Berriasian in age (Figure 9e). It comprises carbonate breccias which they interpreted as the sedimentary response to a regional (?erosive) event at the Jurassic-Cretaceous boundary. The formation was previously thought to be Late Tithonian in age (Chaykovskiy et al., 2006) (Figure 9f), however, and an Upper Tithonian element is permitted by the strontium isotope data and by the fact that they did not sample the base of the formation. Thus the change to brecciated facies may have occurred in Late Tithonian time. A disconformity has not been documented at the base or within the Upper Tithonian Bedenekyr Formation at Demerdzhi (Figure 9h). However, it does contain interbeds of sandstone and conglomerate that might conceivably occur above such a hiatal surface.

In summary, observations from southwest and central Crimea might provide evidence for Late Tithonian disconformity formation. However, when compared with the more robust evidence for an Early Berriasian hiatus above the Bedenekyr Formation in central Crimea (Fikolina et al., 2008) (Figure 9h) and a major tectonic event between the Baydar Formation and Early Cretaceous mudstones in southwest Crimea (Chaykovskiy et al., 2006) this is thought, at best, to be secondary to an intra-Berriasian relative base-level fall. This interpretation is consistent with observations from a number of other regions in Crimea and from the Russian western Greater Caucasus, where Tithonian or Lower Berriasian platform carbonates or evaporates are disconformably overlain by mid/Upper Berriasian or younger sediments (e.g. Bucur et al., 2014; Guo et al., 2011; Korsakov et al., 2004; Korsakov et al., 2002; Nikishin et al., 2015c; Vincent et al., 2016) (Figure 9h-i). Given that sedimentation was also re-established at Kircaova sometime during the latest Tithonian to Berriasian, it is possible that a broadly contemporaneous Berriasian relative base-level fall may have been responsible for all of the approximate Jurassic-Cretaceous boundary stratigraphic gaps discussed above (Figure 9).

Mid/Upper Berriasian to Valanginian sedimentation, largely absent in the Central and Western Pontides, occurred in the western Greater Caucasus and Crimea, as it did in the Eastern Pontides (Figure 9). Individual Hauterivian to Lower Barremian formations in central Crimea are bound by disconformities (Figure 9h), whilst a Late Hauterivian to Early Barremian hiatus occurs in strata in southwest Crimea (Figure 9f). The Upper Hauterivian to Barremian Gubs Formation in the northern western Greater Caucasus also disconformably overlies older strata (Figure 9i). Thus while it is not possible to correlate specific events with those responsible for erosion surfaces B to D at Kircaova, a general phase of discontinuous sedimentation is apparent. Lower Aptian strata are absent from all of the Crimean and Caucasus examples highlighted in this study (Figure 9).

8 Regional implications and conclusions

This study successfully applies strontium isotope stratigraphy to Upper Jurassic-Lower Cretaceous carbonate rocks in the Eastern Pontides for the first time. The combined biostratigraphic and Sr isotope constraints provide greater stratigraphic resolution that was previously available from biostratigraphy alone.

The study indicates that Upper Jurassic-Lower Cretaceous carbonate deposition in the Gümüşhane region of the Eastern Pontides spanned at least the Late Oxfordian to Late Barremian (c. 158-127 Ma). The base of the section may be Callovian in age. Carbonate deposition was interrupted by volcanism during the Late Kimmeridgian, although the presence of volcanic material in underlying sediments (unit III; Koch et al., 2008) suggests that volcanism may have commenced regionally in the Early Kimmeridgian. The hiatus associated with the pronounced incisional surface in the lower part of the succession (erosion surface A) is latest Kimmeridgian to Tithonian or Berriasian in age. Multiple erosion surfaces (B-D) in the upper part of the Kırcaova section were formed sometime during the Hauterivian to Barremian. Meteoric dissolution and karstification is associated with the lava flow and erosion surfaces A to C (Figure 5A, F).

Multiple fluctuations in sea level per stage within the Late Jurassic and Early Cretaceous mean that it is theoretically possible to match each of the relative base-level falls recognised in this study with eustasy (Figure 9). However, the mismatch in the ages of the hiatuses recognised in this study and longer term falls in sea level during the Late Tithonian and, particularly, during the Late Barremian to Early Valanginian (Haq, 2014) (Figure 9) indicate that eustasy was not the main driving mechanism for their formation and that, instead, tectonic controls were probably the driver of relative base-level change.

Dokuz et al. (2017) attributed disconformity formation at erosion surface A at Kırcaova to rebound following slab breakoff after the Cimmerian closure of Paleotethys. This explanation is problematic because this would require (1) the southerly subduction of Paleotethys, north of the eastern Sakarya Zone, and (2) a time lag of at least c. 1-3.5 million years and potentially as much as c. 10-16 million

years between magmatism (which began during deposition of unit III) and relative base-level fall. As Dokuz et al. (2017) conceded, not all tectonic models incorporate southerly subduction and Cimmerian continental collision (e.g. Golonka, 2004; Okay, 2000; Okay and Nikishin, 2015; Pickett and Robertson, 2004; Robertson and Ustaomer, 2012; Robertson et al., 2004; Topuz et al., 2013). More fundamentally, lithospheric modelling suggests that after slab breakoff, uplift will occur before (and not after) surface magmatism (Davies and von Blanckenburg, 1995). Furthermore, isostatic rebound following slab breakoff cannot explain the generation of multiple exposure and erosion surfaces or why shallow-water conditions returned after each emergence event.

Instead, latest Jurassic-Early Cretaceous hiatuses around the Black Sea may be caused by rift-flank uplift during rifting in the Greater Caucasus Basin (Vincent et al., 2016), western Black Sea (Derman, 2002; Nairn and Vincent, 2013) and possibly eastern Black Sea. The age of rifting in the Black Sea is poorly constrained. Intriguingly, however, within the Greater Caucasus Basin subsidence analysis has identified Late Tithonian to Berriasian and Hauterivian to Early Aptian rift events (Vincent et al., 2016) that are within error of the hiatuses identified in this study (Figure 9). If regional extension were the cause, then broad phases of rift-related subsidence and associated rift-flank uplift (rather than near synchronous eustatically-generated events) should be expected. This, along with the inherent imprecision of biostratigraphic determinations and the demonstrable removal of material by erosion, would explain the apparent diachroneity of (i) the initial break-up of the Late Jurassic Berdiga-Inalti-Yalta-Gerpigem carbonate platform around the Jurassic-Cretaceous boundary and (ii) the subsequent recommencement and then interruption of Early Cretaceous sedimentation.

Secondary porosity development associated with the erosion surfaces identified in this study is not extensive. This is possibly due to the relatively fine-grained nature of the inner platform carbonate facies involved. Elsewhere around the Black Sea, however, secondary porosity development during periods of subaerial exposure within higher energy outer platform grainstone, or platform edge or isolated coral boundstone facies is far more pronounced (e.g. Figure 10). Our confirmation of the

likely regional extent of these subaerial exposure surfaces is therefore important for the reduction of exploration risk offshore.

In conclusion, rift-flank uplift may be responsible for hiatus formation in the Kircaova section, Eastern Pontides, although additional work is required to confirm a causal link. If this can be proven, it would enhance our confidence that the disconformities and associated subaerial exposure / karstification events identified in this study will also be developed within carbonate-dominated sediments on the rift-generated Shatskiy Ridge and Mid Black Sea High. This might, in turn, result in the development of intra-carbonate seismic markers and zones of porosity enhancement within this potential reservoir interval in the Black Sea.

Acknowledgements

This paper is dedicated to the memory of the late A. Sami Derman without whom the fieldwork associated with this research would not have been possible. We thank Anne Kelly for her Sr sample preparation, Sarah Sherlock for her Ar-Ar analysis, Fiona Hyden for her siliciclastic petrographic analysis, Marcin Krajewski for useful discussions and John McArthur for permission to use the GTS2012 strontium sea level curve. We also acknowledge the insightful comments of Aral Okay, Anton Kuznetsov and Giovanni Rusciadelli that helped improve the manuscript. The research was funded by CASP's consortium of hydrocarbon exploration companies. RME acknowledges a Hugh Kelly Research Fellowship from Rhodes University, South Africa. The paper is Cambridge Earth Science contribution esc.4078.

References

- Adamia, S.A., Akhvlediani, K.T., Kilasonia, V.M., Nairn, A.E.M., Papava, D., Patton, D.K., 1992. Geology of the Republic of Georgia: a review. *International Geology Review* 34, 447-476, doi: 10.1080/00206819209465614.
- Afanasenkov, A.P., Nikishin, A.M., Obukhov, A.N., 2005. The system of Late Jurassic carbonate buildups in the northern Shatsky swell (Black Sea). *Doklady Earth Sciences* 403, 696-699.
- Afanasenkov, A.P., Nikishin, A.M., Obukhov, A.N., 2007. Eastern Black Sea Basin: Geological Structure and Hydrocarbon Potential. Science World, Moscow (in Russian).
- Altiner, D., Koçyiğit, A., Farinacci, A., Nicosia, U., Conti, M.A., 1991. Jurassic-Lower Cretaceous stratigraphy and paleogeographic evolution of the southern part of north-western Anatolia (Turkey). *Geologica Romana* 27, 13-80.
- Aydın, M., Demir, O., Özçelik, Y., Terzioğlu, N., Satır, M., 1995. A geological revision of Inebolu, Devrekani, Ağlı and Küre areas; new observations in Paleotethys-Neotethys sedimentary successions, in: Erler, A., Ercan, T., Bingöl, E., Örcen, S. (Eds.), *Geology of the Black Sea Region, Proceedings of International Symposium on the Geology of the Black Sea Region*. Mineral Research and Exploration Institute (MTA), Ankara, Turkey, pp. 33-38.
- BouDagher-Fadel, M.K., 2008. *Evolution and Geological Significance of Larger Benthic Foraminifera*. Elsevier, Amsterdam.
- BouDagher-Fadel, M.K., 2012. *Biostratigraphic and Geological Significance of Planktonic Foraminifera*. Elsevier, Amsterdam.
- BouDagher-Fadel, M.K., 2015. *Biostratigraphic and Geological Significance of Planktonic Foraminifera*, 2nd ed. OVPR UCL, London.
- Bucur, I.I., Granier, B., Krajewski, M., 2014. Calcareous algae, microbial structures and microproblematica from Upper Jurassic-lowermost Cretaceous limestones of southern Crimea. *Acta Palaeontologica Romaniae* 10, 61-86.

- Burke, W.H., Denison, R.E., Hetherington, E.A., Koepnick, R.B., Nelson, H.F., Otto, J.B., 1982. Variation of seawater $^{87}\text{Sr}/^{86}\text{Sr}$ through Phanerozoic time. *Geology* 10, 516-519, doi: 10.1130/0091-7613(1982)10<516:VOSSTP>2.0.CO;2.
- Chaykovskiy, B.P., Biletskiy, S.V., Deev, V.B., Demyan, O.S., Krasnorudska, S.I., 2006. Crimea Series sheets L-36-XXVIII (Evpatoriya) & L-36-XXXIV (Sevastopol'), in: Bilets'kiy, S.V. (Ed.), State Geological Map of Ukraine. Ministry of the Environment, State Geological Survey, Kiev, 1:200,000 (in Ukrainian).
- Davies, H.J., von Blanckenburg, F., 1995. Slab breakoff: A model of lithosphere detachment and its test in the magmatism and deformation of collisional orogens. *Earth and Planetary Science Letters* 129, 85-102, doi: 10.1016/0012-821X(94)00237-S.
- Denison, R.E., Koepeck, R.B., Fletcher, A., Howell, M.W., Calloway, W.S., 1994. Criteria for the retention of original seawater $^{87}\text{Sr}/^{86}\text{Sr}$ in ancient shelf limestones. *Chemical Geology: Isotope Geoscience section* 112, 131-143, doi: 10.1016/0009-2541(94)90110-4.
- Derman, A.S., 2002. Black Sea rift sequences. *Türkiye Petrol Jeologları Derneği Bülteni* 14, 36-65.
- Derman, A.S., İztan, Y.H., 1997. Results of geochemical analysis of seeps and potential source rocks from Northern Turkey and the Turkish Black Sea, in: Robinson, A.G. (Ed.), *Regional and Petroleum Geology of the Black Sea and Surrounding Region*. AAPG Memoir, vol. 68, Tulsa, Oklahoma, pp. 313-330, doi: 10.1306/M68612C16.
- Derman, A.S., Sayılı, A., 1995. İnalti Formation; a key unit for regional geology, in: Erler, A., Ercan, T., Bingöl, E., Örcen, S. (Eds.), *Geology of the Black Sea Region, Proceeding of International Symposium on the Geology of the Black Sea Region*. Mineral Research and Exploration Institute (MTA), Ankara, Turkey, pp. 104-108.
- Dokuz, A., Aydınçakır, E., Kandemir, R., Karslı, O., Siebel, W., Derman, A.S., Turan, M., 2017. Late Jurassic magmatism and stratigraphy in the Eastern Sakarya Zone, Turkey: Evidence for the slab breakoff of Paleotethyan oceanic lithosphere. *Journal of Geology* 125, 1-31, doi: 10.1086/689552.

- Dokuz, A., Karsli, O., Chen, B., Uysal, I., 2010. Sources and petrogenesis of Jurassic granitoids in the Yusufeli area, Northeastern Turkey: Implications for pre- and post-collisional lithospheric thinning of the eastern Pontides. *Tectonophysics* 480, 259-279, doi: 10.1016/j.tecto.2009.10.009.
- Dokuz, A., Tanyolu, E., 2006. Geochemical constraints on the provenance, mineral sorting and subaerial weathering of Lower Jurassic and Upper Cretaceous clastic rocks of the Eastern Pontides, Yusufeli (Artvin), NE Turkey. *Turkish Journal of Earth Sciences* 15, 181-209.
- Elderfield, H., 1986. Strontium isotope stratigraphy. *Palaeogeography Palaeoclimatology Palaeoecology* 57, 71-90, doi: 10.1016/0031-0182(86)90007-6.
- Eren, M., 1983. Gümüşhane-Kale Arasının Jeolojisi ve Mikrofasiyes İncelemesi. MSc thesis, Karadeniz Technical University, Trabzon, Turkey (in Turkish).
- Eren, M., Tasli, K., 2002. Kilop Cretaceous hardground (Kale, Gümüşhane, NE Turkey): description and origin. *Journal of Asian Earth Sciences* 20, 433-448, doi: 10.1016/S1367-9120(01)00027-X.
- Fikolina, L.A., Bilokric, O.O., Obshars'ka, N.O., Krasnoruds'ka, S.I., Udovychenko, N.I., 2008. Crimea Series sheets L-36-XXIX (Simferopol) & L-36-XXXV (Yalta), in: Semenenko, V.N. (Ed.), *State Geological Map Ukraine*. Ministry of the Environment, State Geological Survey, Kiev, 1:200,000 (in Ukrainian).
- Golonka, J., 2004. Plate tectonic evolution of the southern margin of Eurasia in the Mesozoic and Cenozoic. *Tectonophysics* 381, 235-273, doi: 10.1016/j.tecto.2002.06.004.
- Gorokhov, I.M., Semikhatov, M.A., Baskakov, A.V., Kut'yavin, E.P., Mel'nikov, N.N., Sochava, A.V., Turchenko, T.L., 1995. Sr isotopic composition in Riphean, Vendian, and Lower Cambrian carbonates from Siberia. *Stratigraphy and Geological Correlation* 3, 1-28.
- Görür, N., 1988. Timing of opening of the Black Sea basin. *Tectonophysics* 147, 247-262, doi: 10.1016/0040-1951(88)90189-8.
- Görür, N., Şengör, A.M.C., Akkök, R., Yılmaz, Y., 1983. Pontidlerde Neo-Tetis'in kuzey kolunun açılmasına ilişkin sedimentolojik veriler (Sedimentological data regarding the opening of the northern branch of Neotethys in the Pontides). *Türkiye Jeoloji Kurumu Bülteni* 26, 11-19 (in Turkish).

Gradstein, F.M., Ogg, J.G., Schmitz, M.D., Ogg, G.M., 2012. A Geologic Time Scale 2012. Elsevier, Oxford, p. 1144.

Guo, L., Vincent, S.J., Lavrishchev, V.A., 2011. Upper Jurassic reefs from the Russian western Caucasus: implications for the Eastern Black Sea. *Turkish Journal of Earth Sciences* 20, 629-653, doi: 10.3906/yer-1012-5.

Haq, B.U., 2014. Cretaceous eustasy revisited. *Global and Planetary Change* 113, 44-58, doi: 10.1016/j.gloplacha.2013.12.007.

Kandemir, R., 2004. Sedimentary characteristics and depositional conditions of Lower-Middle Jurassic Şenköy Formation in and around Gümüşhane. PhD thesis, Karadeniz Technical University, Trabzon, Turkey (in Turkish).

Kandemir, R., Yılmaz, C., 2009. Lithostratigraphy, facies, and depositional environment of the Lower Jurassic Ammonitico Rosso type sediments (ARTS) in the Gümüşhane area, NE Turkey: implications for the opening of the northern branch of the Neo-Tethys Ocean. *Journal of Asian Earth Sciences* 34, 586-598, doi: 10.1016/j.jseaes.2008.08.006.

Kara-Gülbay, R., Ziya Kırmacı, M., Korkmaz, S., 2012. Organic geochemistry and depositional environment of the Aptian bituminous limestone in the Kale Gümüşhane area (NE-Turkey): An example of lacustrine deposits on the platform carbonate sequence. *Organic Geochemistry* 49, 6-17, doi: 10.1016/j.orggeochem.2012.05.006.

Karsli, O., Dokuz, A., Uysal, I., Aydin, F., Kandemir, R., Wijbrans, J., 2010. Generation of the Early Cenozoic adakitic volcanism by partial melting of mafic lower crust, Eastern Turkey: Implications for crustal thickening to delamination. *Lithos* 114, 109-120, doi: 10.1016/j.lithos.2009.08.003.

Kaya, M., Altiner, D., 2015. Microencrusts from the Upper Jurassic–Lower Cretaceous İnaltı Formation (Central Pontides, Turkey): remarks on the development of reefal/peri-reefal facies. *Facies* 61, 1-25, doi: 10.1007/s10347-015-0445-5.

Kaz'min, V.G., Tikhonova, N.F., 2006. Evolution of Early Mesozoic back-arc basins in the Black Sea-Caucasus segment of a Tethyan active margin, in: Robertson, A.H.F., Mountrakis, D. (Eds.), *Tectonic*

Development of the Eastern Mediterranean Region. Geological Society Special Publications, London, vol. 260, pp. 179-200, doi: 10.1144/GSL.SP.2006.260.01.08.

Kazmin, V.G., 2006. Tectonic evolution of the Caucasus and Fore-Caucasus in the Late Paleozoic. Doklady Earth Sciences 406, 1-3.

Kazmin, V.G., Sbortshikov, I.M., Ricou, L.-E., Zonenshain, L.P., Boulin, J., Knipper, A.L., 1986. Volcanic belts as markers of the Mesozoic-Cenozoic active margin of Eurasia. Tectonophysics 123, 123-152, doi: 10.1016/0040-1951(86)90195-2.

Kazmin, V.G., Schreider, A.A., Bulych, A.A., 2000. Early stages of evolution of the Black Sea, in: Bozkurt, E., Winchester, J.A., Piper, J.D.A. (Eds.), Tectonics and Magmatism in Turkey and the Surrounding Area. Geological Society, London, Special Publication, vol. 173, pp. 235-249, doi: 10.1144/GSL.SP.2000.173.01.12.

Ketin, İ., Gümüş, O., 1963. Sinop-Ayancık güneyinde üçüncü bölgeye dahil sahaların jeolojisi hakkında rapor - kısım Jura ve Kretase formasyonlarının etüdü. TPAO Arşivi rap no. 288, Ankara (in Turkish).

Kiessling, W., Flügel, E., Golonka, J., 1999. Paleoreef maps: evaluation of a comprehensive database on Phanerozoic reefs. American Association of Petroleum Geologist Bulletin 83, 1552-1587.

Kırmacı, M.Z., 1992. Alucra-Gümüşhane-Bayburt Yörelerindeki (Dogu Pontid Güney Zonu) Üst Jura-Alt Kretase Yaşlı Berdiga Kireçtası' nın Sedimentolojik incelemesi, Fen Bilimleri Enstitüsü. PhD thesis, Karadeniz Teknik Üniversitesi, Trabzon (in Turkish).

Kırmacı, M.Z., Koch, R., Buccur, I.I., 1996. An Early Cretaceous Section in the Kirchaova Area (Berdiga Limestone, NE - Turkey) and its correlation with Platform Carbonates in W-Slovenia. Facies 34, 1-22, doi: 10.1007/BF02546154.

Koch, R., Bucur, I.I., Kırmacı, M.Z., Eren, M., Tasli, K., 2008. Upper Jurassic and Lower Cretaceous carbonate rocks of the Berdiga Limestone – Sedimentation on an onbound platform with volcanic and episodic siliciclastic influx. Biostratigraphy, facies and diagenesis (Kircaova, Kale-Gümüşhane

area; NE-Turkey). *Neues Jahrbuch für Geologie und Paläontologie, Abhandlungen* 247, 23-61, doi: 10.1127/0077-7749/2008/0247-0023.

Koçyiğit, A., Altiner, D., 2002. Tectonostratigraphic evolution of the North Anatolian palaeorift (NAPR): Hettangian-Aptian passive continental margin of the northern Neo-Tethys, Turkey. *Turkish Journal of Earth Sciences* 11, 169-191.

Konak, N., Okay, A.I., Hakyemez, H.Y., 2009. Tectonics and Stratigraphy of the Eastern Pontides, 2nd International Symposium on the Geology of the Black Sea Region. General Directorate of Mineral Research and Exploration (MTA) / TMMOB, Ankara, Turkey.

Korsakov, S.G., Semenukha, I.N., Beluzhenko, E.V., Chernykh, V.I., Tuzikov, G.R., Grekov, I.I., Tokarev, V.N., Derkachëva, M.G., Sokolov, V.V., 2004. National Geological Map of the Russian Federation, Caucasus series sheet L-37-XXXV (Maykop), 2nd edition ed. St. Petersburg cartographic enterprise of VSEGEI, Moscow, 1:200,000 (in Russian).

Korsakov, S.G., Semenukha, V.M., Andreev, N.M., 2002. National Geological Map of the Russian Federation, Caucasus series sheet L-37-XXXIV (Tuapse), 2nd edition ed. St. Petersburg cartographic enterprise of VSEGEI, Moscow, 1:200,000 (in Russian).

Kuznetsov, A.B., Semikhatov, M.A., Gorokhov, I.M., 2012. The Sr isotope composition of the world ocean, marginal and inland seas: Implications for the Sr isotope stratigraphy. *Stratigraphy and Geological Correlation* 20, 501-515, doi: 10.1134/s0869593812060044.

Leinfelder, R., Schmid, D.U., Nose, M., Werner, W., 2002. Jurassic reef patterns - the expression of a changing globe, in: Kiessling, W., Flügel, E., Golonka, J. (Eds.), *Phanerozoic Reef Patterns*. SEPM, Special Publication, vol. 72, Tulsa, OK, pp. 465-520.

Masse, J.-P., Tüysüz, O., Fenerci-Masse, M., Özer, S., Sari, B., 2009. Stratigraphic organisation, spatial distribution, palaeoenvironmental reconstruction, and demise of Lower Cretaceous (Barremian-lower Aptian) carbonate platforms of the Western Pontides (Black Sea region, Turkey). *Cretaceous Research* 30, 1170-1180, doi: 10.1016/j.cretres.2009.05.004.

- McArthur, J.M., Howarth, R.J., Bailey, T.R., 2001. Strontium Isotope Stratigraphy: LOWESS version 3: best fit to the marine Sr-isotope curve for 0-509 Ma and accompanying look-up table for deriving numerical age. *The Journal of Geology* 109, 155-170, doi: 10.1016/j.cretres.2009.05.004.
- McArthur, J.M., Howarth, R.J., Shields, G.A., 2012. Strontium Isotope Stratigraphy, in: Gradstein, F.M., Ogg, J.G., Schmitz, M.D., Ogg, G.M. (Eds.), *A Geologic Time Scale 2012*. Elsevier, Oxford, pp. 127-144.
- Meisner, A., Krylov, O., Nemcok, M., 2009. Development and structural architecture of the Eastern Black Sea. *The Leading Edge* 28, 1046-1055, doi: 10.1190/1.3236374.
- Nairn, S., Vincent, S.J., 2013. A review of the Cretaceous-Eocene geology of the Turkish margin of the Black Sea. *CASP Black Sea Project report 38*, Cambridge.
- Nikishin, A.M., Okay, A., Tüysüz, O., Demirer, A., Wannier, M., Amelin, N., Petrov, E., 2015a. The Black Sea basins structure and history: new model based on new deep penetration regional seismic data. Part 2: Tectonic history and paleogeography. *Marine and Petroleum Geology* 59, 656-670, doi: 10.1016/j.marpetgeo.2014.08.017.
- Nikishin, A.M., Okay, A.I., Tüysüz, O., Demirer, A., Amelin, N., Petrov, E., 2015b. The Black Sea basins structure and history: new model based on new deep penetration regional seismic data. Part 1: Basins structure and fill. *Marine and Petroleum Geology* 59, 638-655, doi: 10.1016/j.marpetgeo.2014.08.018.
- Nikishin, A.M., Wannier, M., Alekseev, A.S., Almendinger, O.A., Fokin, P.A., Gabdullin, R.R., Khudoley, A.K., Kopaevich, L.F., Mityukov, A.V., Petrov, E.I., Rubtsova, E.V., 2015c. Mesozoic to recent geological history of southern Crimea and the Eastern Black Sea region, in: Sosson, M., Stephenson, R.A., Adamia, S.A. (Eds.), *Tectonic Evolution of the Eastern Black Sea and Caucasus*. Geological Society, Special Publications, London, vol. 428, pp. 241-264, doi: 10.1144/SP428.1.
- Okay, A.I., 1996. Granulite Facies Gneisses from the Pulur Region, Eastern Pontides. *Turkish Journal of Earth Sciences* 5, 55-61.

Okay, A.I., 2000. Was the Late Triassic orogeny in Turkey caused by the collision of an oceanic plateau?, in: Bozkurt, E., Winchester, J.A., Piper, J.D.A. (Eds.), *Tectonics and Magmatism in Turkey and the Surrounding Area*. Geological Society, London, Special Publication, vol. 173, pp. 25-41, doi: 10.1144/GSL.SP.2000.173.01.02.

Okay, A.I., Altiner, D., Sunal, G., Aygöl, M., Akdoğan, R., Altiner, S., Simmons, M., 2017. Geological evolution of the Central Pontides, in: Simmons, M.D., Tari, G.C., Okay, A.I. (Eds.), *Petroleum Geology of the Black Sea*. Geological Society Special Publications, London, vol. 464, doi: 10.1144/SP464.3.

Okay, A.I., Leven, E.J., 1996. Stratigraphy and paleontology of the Upper Palaeozoic sequences in the Pulur (Bayburt) region, Eastern Pontides. *Turkish Journal of Earth Sciences* 5, 145-155.

Okay, A.I., Nikishin, A.M., 2015. Tectonic evolution of the southern margin of Laurasia in the Black Sea region. *International Geology Review* 57, 1051-1076, doi: 10.1080/00206814.2015.1010609.

Okay, A.I., Şahintürk, O., 1997. Geology of the Eastern Pontides, in: Robinson, A.G. (Ed.), *Regional and Petroleum Geology of the Black Sea and Surrounding Region*. AAPG Memoir, vol. 68, Tulsa, Oklahoma, pp. 291-311, doi: 10.1306/M68612C15.

Okay, A.I., Sunal, G., Sherlock, S., Altiner, D., Tüysüz, O., Kylander-Clark, A.R.C., Aygöl, M., 2013. Early Cretaceous sedimentation and orogeny on the active margin of Eurasia: Southern Central Pontides, Turkey. *Tectonics* 32, 1247-1271, doi: 10.1002/tect.20077.

Okay, A.I., Sunal, G., Tuysuz, O., Sherlock, S., Keskin, M., Kylander-Clark, A.R.C., 2014. Low-pressure-high-temperature metamorphism during extension in a Jurassic magmatic arc, Central Pontides, Turkey. *Journal of Metamorphic Geology* 32, 49-69, doi: 10.1111/jmg.12058.

Okay, A.I., Topuz, G., 2017. Variscan orogeny in the Black Sea region. *International Journal of Earth Sciences* 106, 569-592, doi: 10.1007/s00531-016-1395-z.

Okay, A.I., Tüysüz, O., 1999. Tethyan sutures of northern Turkey, in: Durand, B., Jolivet, L., Horváth, F., Séranne, M. (Eds.), *The Mediterranean Basins: Tertiary Extension within the Alpine Orogen*. Geological Society, London, Special Publication, vol. 156, pp. 475-515, doi: 10.1144/GSL.SP.1999.156.01.22.

Pelin, S., 1977. Alucra (Giresun) Güneydoğu Yöresinin Petrol Olanakları Bakımından Jeolojik İncelemesi. PhD thesis, Karadeniz Technical University, Trabzon, Turkey (in Turkish).

Pickett, E.A., Robertson, A.H.F., 2004. Significance of the volcanogenic Nilüfer Unit and related components of the Triassic Karakaya Complex for Tethyan subduction/accretion processes in NW Turkey. *Turkish Journal of Earth Sciences* 13, 97-143.

Robertson, A., Parlak, O., Ustaomer, T., Tasli, K., Inan, N., Dumitrica, P., Karaoglan, F., 2014. Subduction, ophiolite genesis and collision history of Tethys adjacent to the Eurasian continental margin: new evidence from the Eastern Pontides, Turkey. *Geodinamica Acta* 26, 230-293, doi: 10.1080/09853111.2013.877240.

Robertson, A.H.F., Dixon, J.E., 1984. Introduction: aspects of the geological evolution of the Eastern Mediterranean, in: Dixon, J.E., Robertson, A.H.F. (Eds.), *The geological evolution of the Eastern Mediterranean*. Geological Society Special Publication, London, vol. 17, pp. 1-74, doi: 10.1144/GSL.SP.1984.017.01.02.

Robertson, A.H.F., Ustaomer, T., 2012. Testing alternative tectono-stratigraphic interpretations of the Late Palaeozoic-Early Mesozoic Karakaya Complex in NW Turkey: Support for an accretionary origin related to northward subduction of Palaeotethys. *Turkish Journal of Earth Sciences* 21, 961-1007, doi: 10.3906/yer-1003-22.

Robertson, A.H.F., Ustaömer, T., Pickett, E.A., Collins, A.S., Andrew, T., Dixon, J.E., 2004. Testing models of Late Palaeozoic-Early Mesozoic orogeny in Western Turkey: support for an evolving open-Tethys model. *Journal of the Geological Society, London* 161, 501-511, doi: 10.1144/0016-764903-080.

Robinson, A.G., Banks, C.J., Rutherford, M.M., Hirst, J.P.P., 1995. Stratigraphic and structural development of the Eastern Pontides, Turkey. *Journal of the Geological Society, London* 152, 861-872, doi: 10.1144/gsjgs.152.5.0861.

Rud'ko, S.V., Kuznetsov, A.B., Piskunov, V.K., 2014. Sr isotope chemostratigraphy of the Upper Jurassic carbonate rocks in the Demerdzhi Plateau (Crimean Mountains). *Stratigraphy and Geological Correlation* 22, 494-506.

Rud'ko, S.V., Kuznetsov, A.B., Pokrovsky, B.G., 2017. Sr chemostratigraphy, $\delta^{13}\text{C}$, and $\delta^{18}\text{O}$ of rocks in the Crimean carbonate platform (Late Jurassic, Northern Peri-Tethys). *Lithology and Mineral Resources* 52, 479-497.

Şengör, A.M.C., Yılmaz, Y., 1981. Tethyan evolution of Turkey: a plate tectonic approach. *Tectonophysics* 75, 181-241, doi: 10.1016/0040-1951(81)90275-4.

Taslı, K., 1997. Stratigraphical and paleontological data on the Malm volcanism in the eastern Pontides (NE Turkey). *Istanbul University Earth Sciences Bulletin* 8, 95-101 (in Turkish).

Taslı, K., Özer, E., Yılmaz, C., 1999. Biostratigraphic and environmental analysis of the Upper Jurassic-Lower Cretaceous carbonate sequence in the Basoba Yayla area (Trabzon, NE Turkey). *Turkish Journal of Earth Sciences* 8, 125-135.

Taslı, K., Özsayar, T., 1997. Stratigraphy and paleoenvironmental setting of the Albian-Campanian carbonate sequence in the Gümüşhane province (Eastern Pontides, NE Turkey). *TAPG Bulletin* 9, 13-29 (in Turkish).

Tokel, S., 1972. Stratigraphical and volcanic history of the Gümüşhane region, NE Turkey. PhD thesis, University College London, UK.

Topuz, G., Altherr, R., Kalt, A., Satır, M., Werner, O., Schwarz, W.H., 2004a. Aluminous granulites from the Pulur complex, NE Turkey: a case of partial melting, efficient melt extraction and crystallisation. *Lithos* 72, 183-207, doi: 10.1007/s00531-003-0372-5.

Topuz, G., Altherr, R., Satır, M., Schwarz, W., 2004b. Low-grade metamorphic rocks from the Pulur complex, NE Turkey: implications for the pre-Liassic evolution of the Eastern Pontides. *International Journal of Earth Sciences* 93, 72-91, doi: 10.1016/j.lithos.2003.10.002.

- Topuz, G., Altherr, R., Schwarz, W., Dokuz, A., Meyer, H.-P., 2007. Variscan amphibolite-facies rocks from the Kurtoğlu metamorphic complex (Gümüşhane area, Eastern Pontides, Turkey). *International Journal of Earth Sciences* 96, 861-873, doi: 10.1007/s00531-006-0138-y.
- Topuz, G., Altherr, R., Siebel, W., Schwarz, W.H., Zack, T., Hasözbek, A., Barth, M., Satlr, M., Sen, C., 2010. Carboniferous high-potassium I-type granitoid magmatism in the Eastern Pontides: The Gümüşhane pluton (NE Turkey). *Lithos* 116, 92-110, doi: 10.1016/j.lithos.2010.01.003.
- Topuz, G., Göçmengil, G., Rolland, Y., Çelik, Ö.F., Zack, T., Schmitt, A.K., 2013. Jurassic accretionary complex and ophiolite from northeast Turkey: No evidence for the Cimmerian continental ribbon. *Geology* 41, 255-258, doi: 10.1130/g33577.1.
- Tüysüz, O., 1990. Tectonic evolution of a part of the Tethyside orogenic collage: the Kargı Massif, northern Turkey. *Tectonics* 9, 141-160, doi: 10.1029/TC009i001p00141.
- Ustaömer, T., Robertson, A.H.F., 2010. Late Palaeozoic-Early Cenozoic tectonic development of the Eastern Pontides (Artvin area), Turkey: stages of closure of Tethys along the southern margin of Eurasia, in: Sosson, M., Kaymakci, N., Stephenson, R.A., Bergerat, F., Starostenko, V. (Eds.), *Sedimentary basin tectonics from the Black Sea and Caucasus to the Arabian Platform*. Geological Society, London, Special Publication, vol. 340, pp. 281-327, doi: 10.1144/SP340.13.
- Vincent, S.J., Braham, W., Lavrishchev, V.A., Maynard, J.R., Harland, M., 2016. The formation and inversion of the western Greater Caucasus Basin and the uplift of the western Greater Caucasus: Implications for the wider Black Sea region. *Tectonics* 35, 2948-2962, doi: 10.1002/2016TC004204.
- Yılmaz, C., 1992. Kelkit (Gümüşhane) Yöresinin Stratigrafisi. *Jeoloji Mühendisliği Dergisi* 40, 50-62 (in Turkish).
- Yılmaz, C., 2002. Tectono-sedimentary records and controlling factors of the Mesozoic sedimentary basin in the Gümüşhane-Bayburt region. *Türkiye Jeoloji Bülteni* 45, 141-164 (in Turkish).
- Yılmaz, C., Kandemir, R., 2006. Sedimentary records of the extensional tectonic regime with temporal cessation: Gümüşhane Mesozoic Basin (NE Turkey). *Geologica Carpathica* 57, 3-13.

Yılmaz, Y., Tüysüz, O., Yiğitbaş, E., Can Genç, S., Şengör, A.M.C., 1997. Geology and tectonic evolution of the Pontides, in: Robinson, A.G. (Ed.), *Regional and Petroleum Geology of the Black Sea and Surrounding Region*. AAPG Memoir, vol. 68, Tulsa, Oklahoma, pp. 183-226, doi: 10.1306/M68612C11.

Table captions

Table 1. Summary of the stratigraphic units identified in the Middle or Upper Jurassic to Lower Cretaceous Kircaova section in the Eastern Pontides (locality PT09_21E).

Table 2. Micropaleontological analyses of selected thin sections from locality PT09_21 in the Eastern Pontides. Ages are based on first appearance Planktonic Foraminiferal zones, Shallow Benthic zones and letter stages after BouDagher-Fadel (2008, 2012, 2015). See Figure 2 and Figure 4 for their location.

Table 3. Sample ages derived from the Sr isotope seawater curve (McArthur et al., 2012), using foraminiferal data from the same section and stratigraphic position to discriminate between multiple possible positions on the curve. Minimum and maximum age uncertainty is calculated to include both the analytical error (2σ) and the uncertainty on the seawater curve. Note that the stratigraphic height relative to the base of section does not always correspond to stratigraphic position because of the relief on the erosion surface. See Figure 2 and Figure 4 for their location.

Table 4. Micropaleontological analyses of selected thin sections from the section south of Küre at locality PT09_017 (41.70450°N, 33.69394°E) in the Central Pontides. Ages are based on first appearance Planktonic Foraminiferal zones, Shallow Benthic zones and letter stages after BouDagher-Fadel (2008, 2012, 2015).

Figure captions

Figure 1. Tectonic map of the Black Sea region showing eastern Sakarya and the Kircaova section in its regional context. Modified from Okay and Tüysüz (1999). Abbreviations: AM = Ağvanis Massif; PM = Pulur Massif; ATB = Adjara-Trialet Belt.

Figure 2. Panorama of Upper Jurassic – Lower Cretaceous strata at Kircaova (locality PT09_21E) with sample positions, the stratigraphic subdivisions of Koch et al. (2008) and the four erosion surfaces (A-D) and lava flow marked. The field of view is located on Figure 3.

Figure 3. Geological map showing the outcrop pattern of the Berdiga Formation to the south of Kale in the Gümüşhane region of the Eastern Pontides. The main logged section at locality PT09_21E is known as the Kircaova section after the previous work of Koch et al. (2008). Additional information and samples were collected from the lower part of the formation at locality PT09_21B. These were correlated using the lava flow at 70 m in the logged section (Figure 4). The base of the section was also observed at locality PT09_21A. Modified from Kandemir (2004) and Karsli et al. (2010).

Figure 4. Summary stratigraphy of locality PT09_21 in the Eastern Pontides showing the main facies, the key erosional / subaerially exposed surfaces and the strontium and *in situ* foraminiferal age ranges. The strontium age uncertainties include both the analytical error (2σ) and the uncertainty on the seawater curve (see Figure 8). The maximum and minimum permitted age ranges of the hiatuses (light and dark grey shading, respectively) are based on the age uncertainties of the samples that bracket the hiatuses. Note that the Sr-derived ages are much more precise than those provided by the foraminiferal ages alone. Samples are located on Figure 2. The stage boundaries are from Gradstein et al. (2012).

Figure 5. Typical carbonate facies in thin section from Upper Jurassic – Lower Cretaceous strata at Kircaova (locality PT09_21E) in the eastern Pontides. A) Large bivalve shells within a gastropod floatstone. Note the occurrence of pendant cement lining an early dissolved bivalve shell (black

arrow) that is indicative of meteoric dissolution and cementation in a vadose environment. Also note the micritic envelopes (white arrow) and blocky spar calcite cement (b). Sample 21E_02. B) Lime mudstone; note the ostracod (black arrow) and rare dolomite crystals (white arrow). Sample 21B_03. C) Dolostone whose original texture is completely altered by fine-grained dolomite with scattered dissolution vugs. Sample 21E_14. D) Intraclastic-bioclastic grainstone facies comprising intraclasts (bioclastic limestones) and abundant small benthic foraminifera and bivalves. Note the pore spaces filled with isopachous (black arrow) and drusy (d) calcite cements. Sample 21E_17. E) Foraminifera packstone-grainstone facies with abundant small (miliolids) and large benthic foraminifera in a partly grain- and partly mud-supported matrix. Sample 21E_23. Unlike other samples in units X-XII, this sample has not been affected by dolomitisation. F) Limestone clasts from the erosion surface C are cemented by clays in a meniscus style (black arrow), which was formed in a vadose environment. Sample 21E_28.

Figure 6. Field photographs of the erosion surfaces A-D within Upper Jurassic – Lower Cretaceous strata at Kircaova (locality PT09_21E). A) Relief on erosion surface A on the northwestern margin of its incised valley. B) Approximately 45 m of relief on erosion surface A on the southeastern margin of its incised valley. C) Brecciated limestones at the top of unit V at erosion surface A. D) Erosion surface B overlain by sandstones, laminated limestones and limestone breccias. E) Detail of the micrite-cemented limestone breccia above erosion surface B. F) Erosion surface C overlain by limestone conglomerates with clasts up to 10 cm in diameter. G) Erosion surface D overlain by poorly cemented limestone breccias, which include reworked calcrete peds, and laminated limestones. See Figure 2 and Figure 4 for the wider context of these erosion surfaces.

Figure 7. Selected foraminiferal photomicrographs of samples from locality PT09_21. 1) *A-Debarina hahounerensis* Forcade, Raoult and Vila, B-*Vercorsella arenata* Arnaud-Vanneau, Sample 21E_33, x30. 2) *Pseudolituonella gavonensis* Foury, Sample 21E_33, x20. 3) *Debarina hahounerensis* Forcade Sample 21E_33, x15. 4-5) *Vercorsella arenata* Arnaud-Vanneau, 4, Sample 21E_33; 5, Sample

S_PT09_SV_21E_27, x30. 6) *Praechrysalidina infracretacea* Luperto Sinni, Sample 21E_27, x18. 7) *Andersenolina elongata* (Leupold), Sample 21E_16, x56. 8) *A-Cuneolina camposaurii* Sartoni and Crescenti. *B-Andersenolina elongata* (Leupold), Sample 21E_17, x20. 9) *A-Andersenolina elongata* (Leupold). *B-Praechrysalidina infracretacea* Luperto Sinni, Sample 21E_16, x28. 10-11) *Pseudocyclammina lituus* (Yokoyama) Sample 21E_02, 10, x28; 11, x32. 12) *Rectocyclammina chouberti* Hottinger, Sample 21E_02, x22. 13-14) *Alveosepta jaccardi* (Schrodt), Sample 21E_02, 13, x45; 14, x58. 15) *Pseudocyclammina* sp., Sample 21E_02, 13, x20. 16) *Mesoendothyra* sp., Sample 21E_02, x60. 17) *Trocholina conica* (Schlumberger), Sample 21B_08, x80.

Figure 8. Measured Sr isotope ratio and analytical error (2σ) of the samples in this study plotted against best age estimate and its uncertainty as derived from the Sr isotope seawater curve (McArthur et al., 2012). Insert illustrates that multiple ages can be interpreted from the Sr isotope seawater curve between 100-200 Ma. The most likely ages have been identified on the basis of combined foraminiferal data from the same section and the relative stratigraphic position of the samples. The stage boundaries are from Gradstein et al. (2012).

Figure 9. Correlation diagram of selected Upper Jurassic – Lower Cretaceous strata in the Eastern Black Sea region, highlighting possible common hiatus age ranges and their potential driving mechanisms. The sections are located on Figure 1.

Figure 10. Examples of meteoric dissolution porosity in Late Jurassic carbonates from the Black Sea region. A) Lithoclastic oolitic grainstone from the Late Tithonian Bedenekyr Formation at locality CR35 in central Crimea showing oomouldic secondary porosity (black arrow). B) Reef boundstones from the Late Tithonian Baydar Formation at locality CR54 in southwest Crimea showing dissolution vugs largely filled by differing generations of phreatic cements (black arrow). Sample localities are shown on Figure 1.

Koch et al. (2008)							
ACCEPTED MANUSCRIPT							
Koch et al. (2008)				This work			
Stratigraphic unit	Thickness (m)	Description	Interpretation	Age range	Thickness (m)	Additional comments	Reinterpreted maximum age range
XVI	23	Interbedded intraclastic, foraminiferal wackestones, packstones and grainstones.	Low-energy intertidal to high-energy shallow normal marine conditions.	Barremian		Not observed.	
XV	20	Thick to very thick bedded packstones-grainstones interbedded with medium to thick bedded lime mudstones to wackestones with algal laminations and birdseye structures.	Moderate- to high-energy, shallow to intertidal normal marine conditions.	Hauterivian	>19	Thick bedded bioclastic packstones and grainstones with minor lime mudstone interbeds.	Late Barremian to Early Aptian
XIV	20	Thick bedded intraclastic-foraminiferal-dasycladial packstones-grainstones with four thin intercalated siliciclastic layers containing volcanic rock fragments.	Alternating low- and high-energy normal marine conditions.	Late Valanginian - Early Hauterivian	24	Contains erosion surfaces C & D. Each surface is overlain by reddened breccia-conglomerates (clasts). Clay filled fissures occur below surface C. Other lithologies include sandstone, foraminifera packstone-grainstone, mollusc floatstone, intraclastic and bioclastic grainstone, bioclastic wackestone, lime mudstones and laminated stromatolites.	Early Hauterivian to Late Barremian
XIII	3	Dolomite overlain by a 70 cm thick conglomerate.	Low-energy conditions.	Late Valanginian			
XII	10	Medium to thick bedded intraclastic-foraminiferal-dasycladial packstones-grainstones interbedded with dolomitic limestone and dolomite.	High-energy conditions.	Late Valanginian	57	Medium- to thick-bedded intraclastic and bioclastic wackestones, packstones and grainstones that have undergone varying amounts of dolomitization. Capped by erosion surface B.	Early Hauterivian
XI	12	Medium bedded fine- to medium-crystalline dolomite.	?Low- to moderate-energy conditions.	Early Valanginian			
X	13	Medium to thick bedded, partially dolomitised, gastropod-rich intraclastic-foraminiferal packstones-grainstones.	High-energy conditions.	Earliest Valanginian			
IX	31	Medium to thick bedded, partially dolomitised, intraclastic-foraminiferal packstone-grainstones.	?Low- to moderate-energy conditions.	Berriasian	30	Medium- to thick-bedded, dolomitized bioclastic wackestones.	Early Hauterivian
VIII	4	Medium to thick bedded, dolomitic intraclastic, oolitic and foraminiferal packstones and grainstones.	High-energy (open) shallow-water environment.	Earliest Berriasian	5	Medium- to thick-bedded intraclastic and bioclastic, coated grain packstones and grainstones.	Late Valanginian to Early Hauterivian
VII	36	4 m of in situ fine- to medium-crystalline dolomite. Slope debris composed of micritic limestones.	Low-energy environment.	Latest Tithonian	57	Dolostones	Early Valanginian to Early Hauterivian
VI	30	Medium to thick bedded lime mudstones. The lower 8 m are reported to be Kimmeridgian.	Low-energy, restricted environment.	Latest Kimmeridgian-Tithonian	17-62	Lower 45 m thick incised valley fill (not recognised by Koch <i>et al.</i> , 2008) comprises limestone breccias, conglomerates, sandstones (volcanic lithic arkoses) and dolostones. Valley shoulder sediments comprise thick bedded dolostones.	Early Berriasian to Early Hauterivian
V	43	Thick bedded lime mudstones that are locally brecciated, with local biomicrites.	Low-energy, restricted environment.	Late Kimmeridgian	9-54	Thick bedded lime mudstones. The uppermost sediments are brecciated and karstified and capped by erosion surface A with up to 45 m of local relief.	Late Kimmeridgian
IV	10	Heavily weathered 'diabase sill' that includes single large pillows.	Submarine extrusion.	Middle Kimmeridgian	10	Highly weathered doleritic lava flow. Pillow structures and entrained limestones suggest subaqueous eruption. Capped by tuffaceous siltstones and reddish mudstones deposited in a nearshore to subaerial environment.	?Late Kimmeridgian
III	23	Medium to thick bedded micritic limestones with local algal laminations and only minor biogenic components. Contains reworked volcanic rock fragments and evidence for subaerial exposure.	Restricted platform interior. Contemporaneous volcanic activity.	Late Oxfordian to Early Kimmeridgian	23	Medium to thick bedded dolostones passing up into lime mudstones. Subaerial dissolution surface at top.	Late Oxfordian to Kimmeridgian or Kimmeridgian
II	29	Medium bedded fine- to medium- and thick to very thick bedded medium- to coarse-crystalline dolomites. Ghosts of foraminifera, ooids, oncoids and peloids.	Moderate-energy, more restricted platform conditions.	Middle to Late Oxfordian	29	Medium to thick bedded dolostones.	Callovian to Late Oxfordian or Late Oxfordian to Early Kimmeridgian
I	18	Medium bedded wackestone-packstone and very thick bedded packstone-grainstone interbeds. Microbial oncoids are characteristic. Intraclasts include coral and agglutinated foraminifera.	Moderate- to high-energy, open marine platform conditions.	Early Oxfordian	18	Very thick bedded intraclastic and bioclastic packstones, and grainstones.	Callovian to Early Oxfordian or Middle Oxfordian to earliest Kimmeridgian

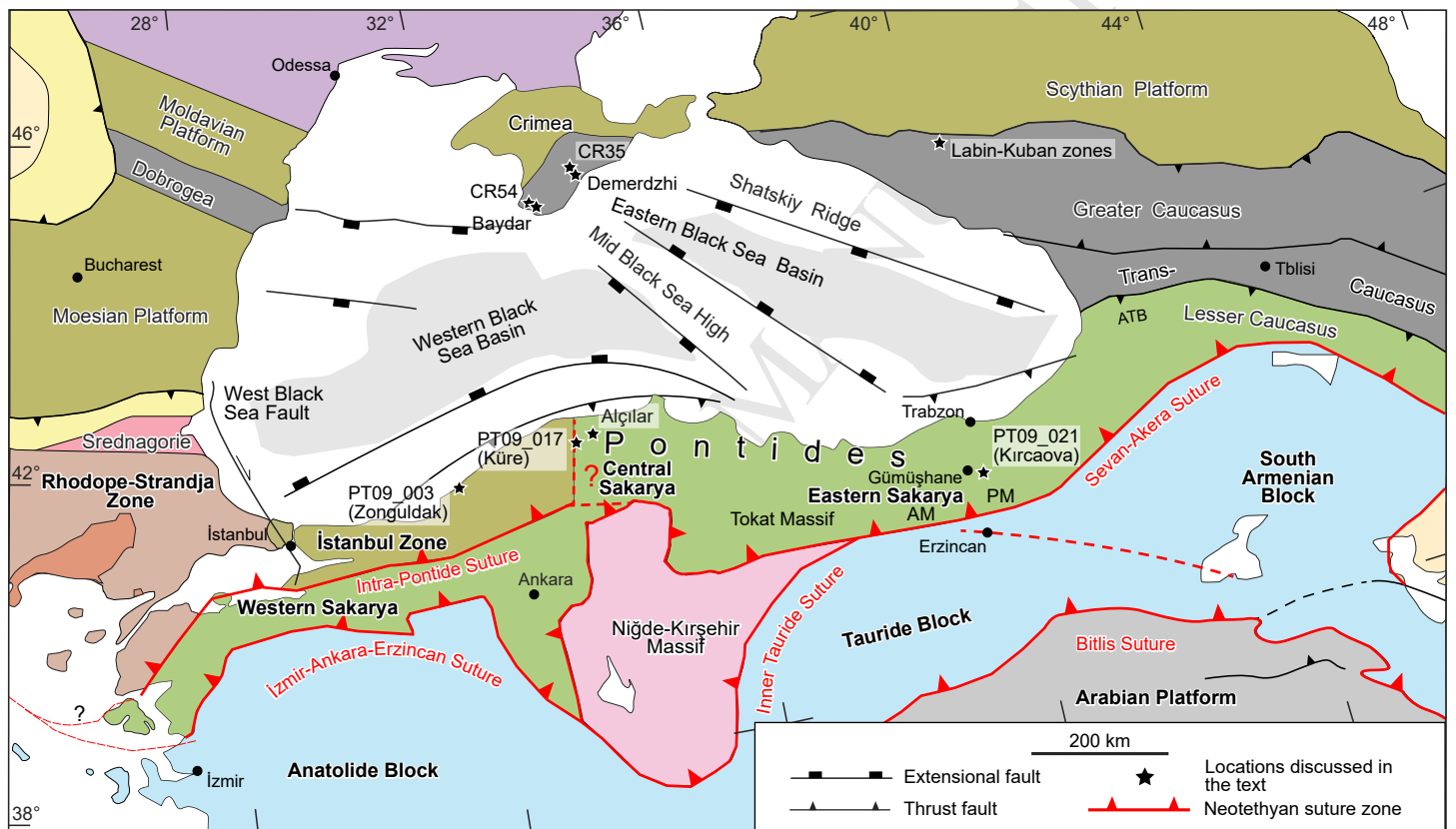
Sample number	Height (m)	Stratigraphic unit	Biological components	Depositional environment	Determined age
21E_33	331	XV	<i>Arenobulimina</i> sp., miliolid spp., <i>Lituola</i> sp., <i>Pseudolituonella gavonensis</i> , <i>Pseudopfenderina neocomiensis</i> , <i>Vercorsella arenata</i> , <i>Cuneolina laurenti</i> , <i>Debarina hahounerensis</i> , Dasyclad spp. (<i>Cylindroporella</i> sp.)	Low energy restricted environment	Late Barremian - Aptian (Late Barremian based on first occurrence of <i>Debarina</i> sp.)
21E_31	325		Small miliolids, <i>Cuneolina</i> sp., <i>Vercorsella</i> sp., Dasyclad spp. (<i>Cylindroporella</i> sp.)		
21E_30	320.5	XIII-XIV	Small miliolids		
21E_29	316		Small miliolids, ? <i>Cuneolina</i> sp.		
21E_28	309		Small miliolids, <i>Pseudocyclammina</i> sp., <i>Textularia</i> sp., <i>Everticyclammina</i> sp., <i>Everticyclammina virguliana</i>		
21E_27	303		Small miliolids, <i>Pseudocyclammina</i> sp., <i>Textularia</i> sp., <i>Everticyclammina</i> sp., <i>Buccicrenata</i> sp., <i>Praechrysalidina infracretacea</i> , <i>Vercorsella arenata</i> , <i>Pfenderina neocomiensis</i> , Dasyclad spp. (<i>Cylindroporella</i> sp.)		Hauterivian - Aptian (Hauterivian based on the first occurrence of <i>Praechrysalidina infracretacea</i> and <i>Vercorsella arenata</i>)
21E_23	294.5	X-XII	Small miliolids, <i>Textularia</i> sp., <i>Pfenderina</i> spp., <i>Ammobaculites</i> sp., <i>Textularia</i> sp., <i>Buccicrenata</i> sp., Dasyclad spp.		
21E_21	254.5		Small miliolids, <i>Textularia</i> sp.		
21E_20	238	IX	Small miliolids		
21E_19	227		Small miliolids, <i>Textularia</i> sp., <i>Riyadhoides</i> sp. (reworked), <i>Andersenolina elongata</i> , Dasyclad spp., Gastropod spp.		
21E_18	217.5		Small miliolids, <i>Textularia</i> sp., <i>Riyadhoides</i> sp. (reworked), <i>Andersenolina elongata</i> , Dasyclad spp., Gastropod spp.		

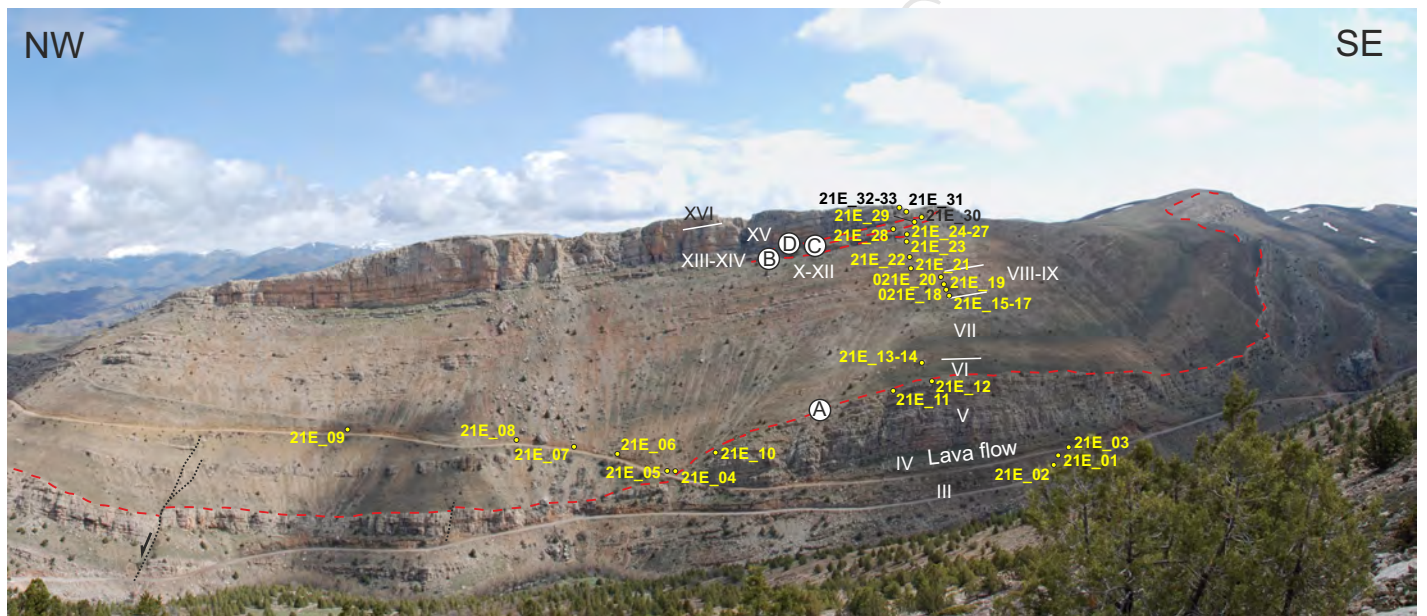
21E_17	212.5	VIII	Small miliolids, <i>Textularia</i> sp., <i>Riyadhoides</i> sp. (reworked), <i>Everticyclammina</i> sp., <i>Kastamonina abanica</i> (reworked), <i>Andersenolina elongata</i> , <i>Cuneolina camposaurii</i> , <i>Dasyclad</i> spp., <i>Gastropod</i> spp.	Hauterivian - Aptian assemblage based on <i>Cuneolina camposaurii</i>
21E_16	211.5		Small miliolids, <i>Textularia</i> sp., <i>Riyadhoides</i> sp., <i>Andersenolina elongata</i> , <i>Praechrysalidina infracretacea</i> , <i>Protpeneroplis</i> sp., <i>Dasyclad</i> sp.	?Kimmeridgian - Tithonian (<i>Riyadhoides</i> a Late Jurassic form but maybe reworked)
21E_15	209.5		Small miliolids, <i>Textularia</i> sp., <i>Pseudomarssonella</i> sp., <i>Protpeneroplis</i> sp., <i>Pfenderina</i> sp., <i>Andersenolina elongata</i> , <i>Riyadhoides</i> sp., <i>Dasyclad</i> sp.	?Kimmeridgian - Tithonian (<i>Riyadhoides</i> a Late Jurassic form but maybe reworked as above)
21E_05	101	VI	<i>Dasyclads</i> algae	
21E_01	67.5	III	<i>Streptocyclammina parvula</i> , <i>Everticyclammina virguliana</i> , <i>Gastropod</i> spp.	Kimmeridgian
21E_02	65		<i>Alveosepta jaccardi</i> , <i>Pseudocyclammina lituus</i> , <i>P.</i> sp., <i>Rectocyclammina chouberti</i> , <i>Mesoendothyra</i> sp., <i>Everticyclammina</i> sp., <i>Buccicrenata</i> sp., <i>Gastropod</i> spp., <i>Dasyclad</i> spp.	Early - early Late Kimmeridgian
21B_08	15	I	<i>Trocholina conica</i> , <i>Neotrocholina</i> sp., <i>Textularia</i> spp., <i>Nautiloculina</i> sp.	Bathonian - Oxfordian
HUR9	14		<i>Trocholina conica</i> , <i>Trocholina</i> cf. <i>solecensis</i>	Callovian-Oxfordian
HUR8	8		<i>Protpeneroplis striata</i> , <i>Trocholina conica</i> , <i>Neotrocholina</i> sp., <i>Textularia</i> spp., <i>Nautiloculina</i> sp.	Bathonian-Oxfordian
HUR6	2		Recrystallised algae, ? <i>Protpeneroplis striata</i>	?Bathonian-Berriasian

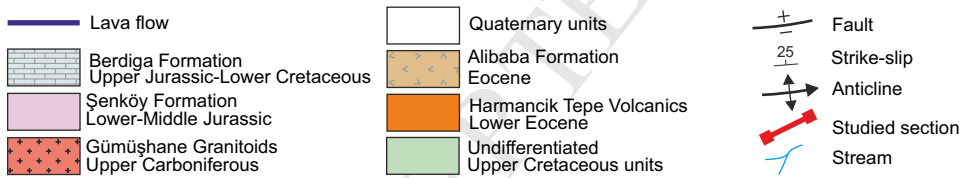
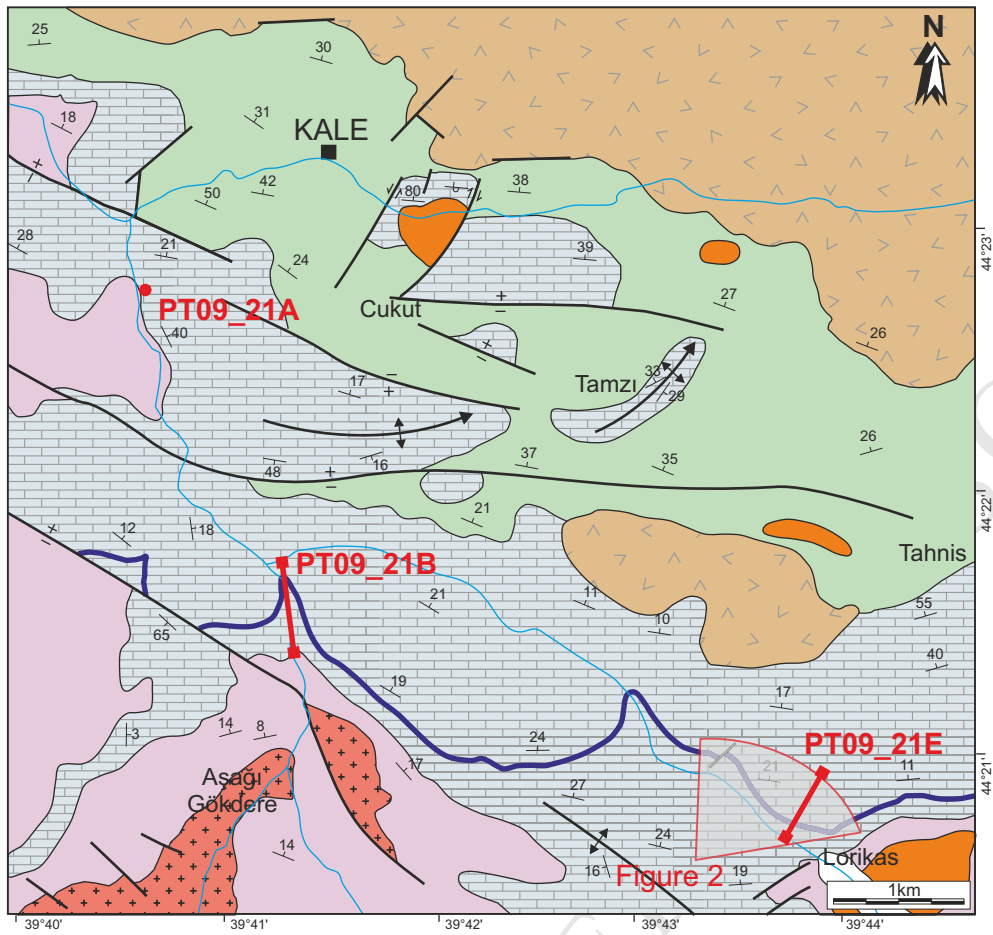
Sample number	Comment on sample	Height (m)	Stratigraphic unit	Position relative to erosion surfaces	Sr isotope ratio	2 sigma error	Max age (Ma)	Min age (Ma)	Comment on age interpretation
21E_32	difficult to avoid vein	329.5	XV	above D	0.707447	0.000024	127.95	125.95	Several possible ages but only one that is compatible with the overlying foram data and stratigraphic position
21E_30 rudist	rudist	320.5	XIII-XIV	above D	0.707486	0.000032	131.90	126.90	Only the lower error range intersects with the sea level curve
21E_30 infill	mcrite infill	320.5		above D	0.707512	0.00003	130.10	128.10	Only the lower error range intersects with the sea level curve
21E_29		316		above D	0.707420	0.000028	133.65	131.85	Several possible ages but only one that is compatible with the foram data and stratigraphic position. Within error of the stratigraphically lower 21E_27, which constraints the ages of both these samples to the area of overlapping errors. Note however, the erosion surface that separates the two.
21E_28		309		between C & D	0.7075283	0.000036			Ages not stratigraphically compatible
21E_27		303		between B & C	0.707442	0.000028	132.80	131.25	Several possible ages but only one that is compatible with the foram data and stratigraphic position. Within error of the stratigraphically higher 21E_29, which constraints the ages of both these samples to the area of overlapping errors. Note however, the erosion surface that separates the two.
21E_23	bivalve	294.5	X-XII	between A & B	0.707377	0.000026	137.00	133.10	Several possible ages but only one that is compatible with the overlying foram data and stratigraphic position
21E_17		212.5	VIII	between A & B	0.707368	0.00003	137.65	133.25	Several possible ages but only one that is compatible with the stratigraphic position and foram data
21E_14		153	VII	between A & B	0.707365	0.000028	137.70	133.35	Several possible ages but only one that is compatible with the stratigraphic position
21E_12		132	V	below A	0.706987	0.000028	154.25	152.35	Two possible ages: the younger is compatible with the foram data below. Within error of the stratigraphically lower 21E_11, which constraints the ages of both these samples to the area of overlapping errors.

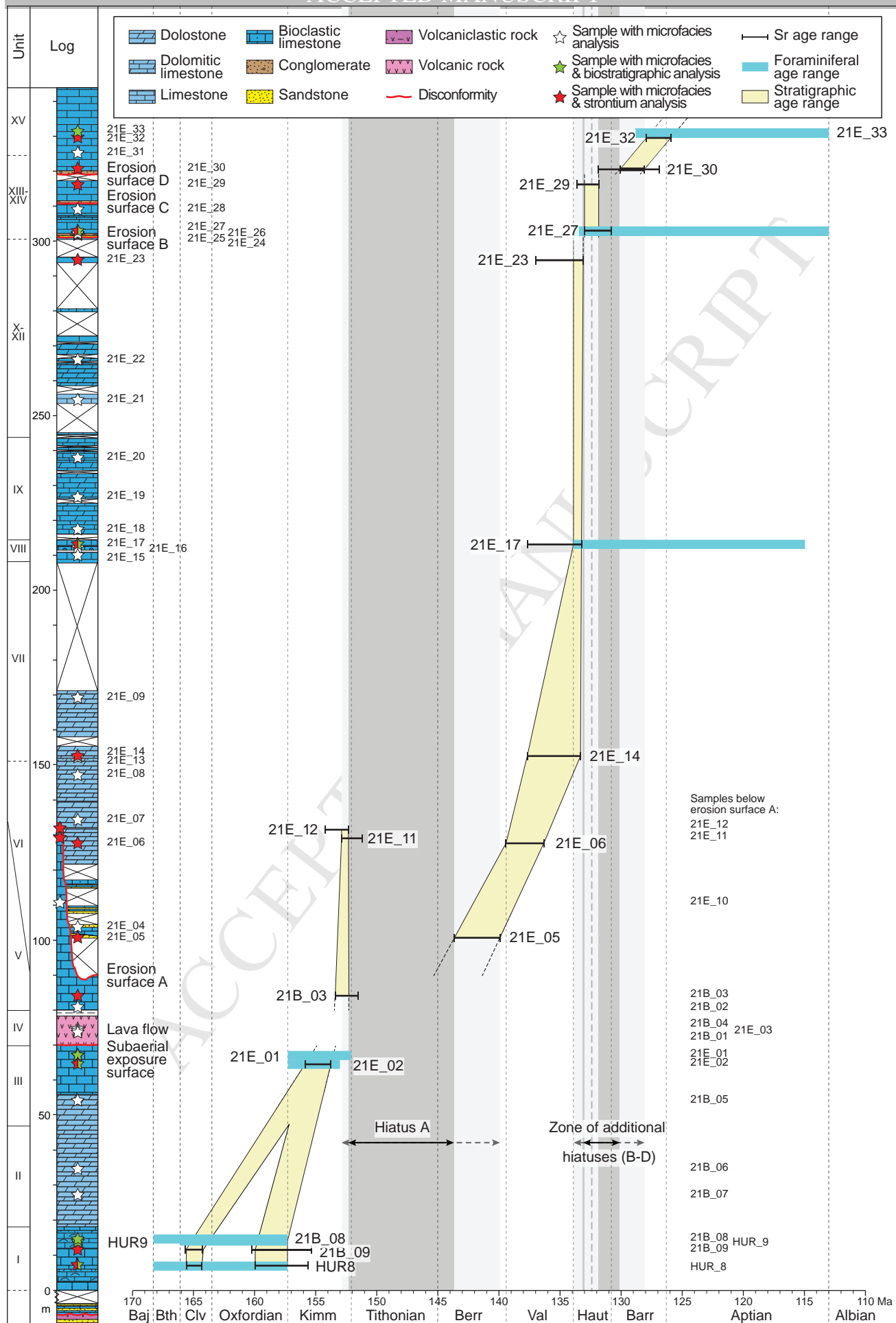
21E_11	micrite	129.5		below A	0.707028	0.000024	152.90	151.20	Two possible age ranges. The younger one is compatible with both the foram data below. Within error of the stratigraphically higher 21E_12, which constrains the ages of both these samples to the area of overlapping errors.
21E_06		128	VI	between A & B	0.707324	0.00003	139.45	136.35	Several possible ages but only one that is compatible with the stratigraphic position
21E_05	micrite	101		between A & B	0.707246	0.000032	143.70	139.95	Several possible ages but only one that is compatible with the stratigraphic position
21B_03	Lime mudstone	84.5	V	below A	0.707013	0.000028	153.45	151.50	Two possible age ranges. The younger one is compatible with both the foram data and stratigraphic position
21E_02	brachiopod	65	III	below A	0.706940	0.000026	155.90	153.80	Two possible age ranges. The younger one is compatible with both the foram data and stratigraphic position
21B_08	difficult to avoid vein	15	I	below A	0.707528	0.000028			Not stratigraphically compatible; probably diagenetically altered as a result of vein carbonate
HUR9		14		below A	0.707857	0.000028			Ages not stratigraphically compatible
21B_09		12		below A	0.706887	0.00003	160.25	155.35	Two possibilities due to inflection point in the seawater curve
					0.706887	0.00003	165.70	164.25	
HUR8		8		base of section	0.706885	0.000026	159.95	155.60	Two possibilities due to inflection point in the seawater curve
					0.706885	0.000026	165.60	164.30	

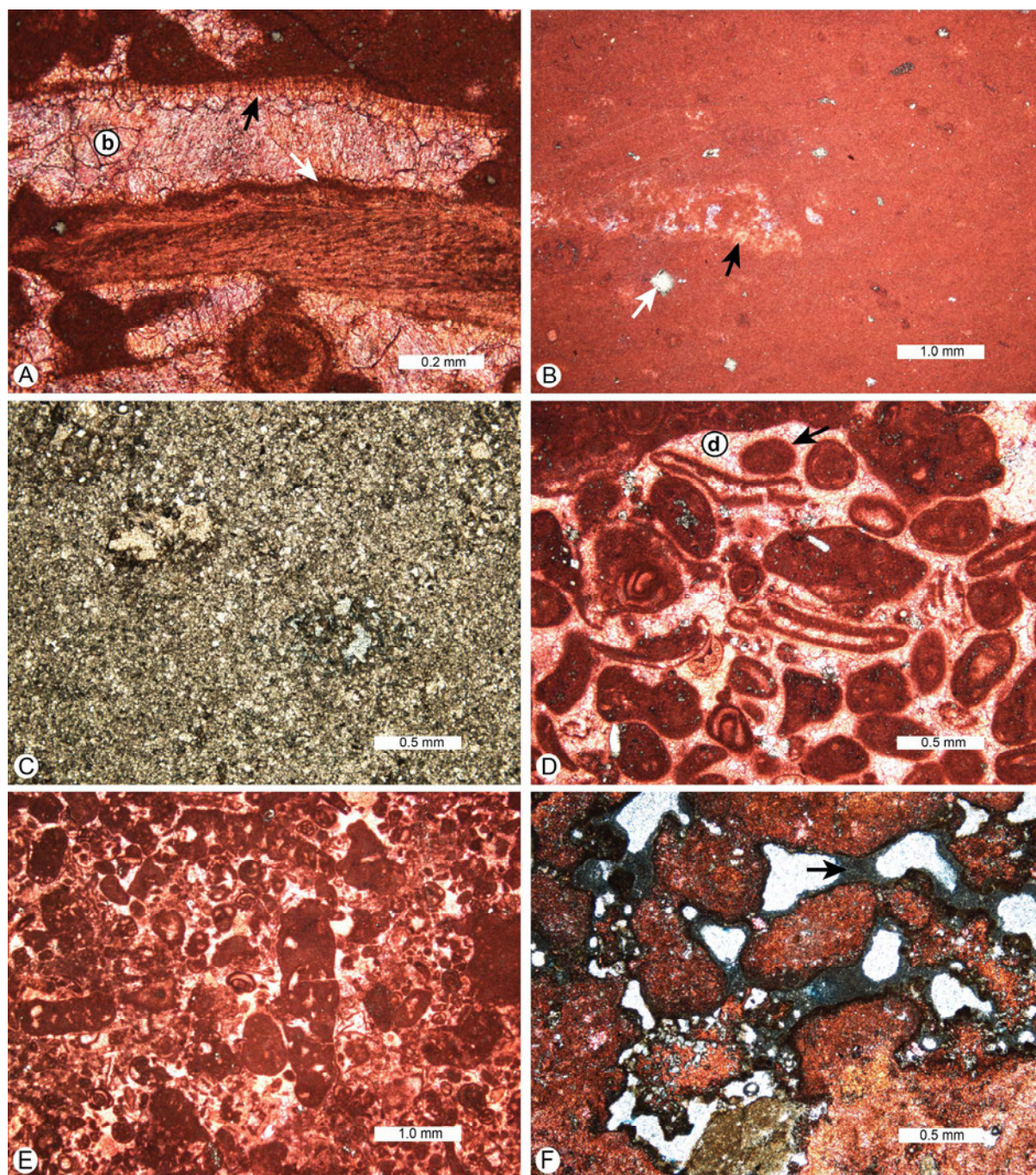
Sample number	Height (m)	Biological components	Determined age
17_16	111.5	<i>Pseudocyclammina lituus</i>	Callovian-Tithonian (Kimmeridgian-Tithonian because of underlying sample)
17_15	108.5	<i>Pseudocyclammina lituus</i> , <i>Pseudocyclammina</i> sp., <i>Everticyclammina</i> sp., <i>Cladocoropsis mirabilis</i>	Kimmeridgian-Tithonian
17_14	102.5	<i>Cladocoropsis mirabilis</i>	Callovian-Tithonian (Kimmeridgian-Tithonian because of underlying sample)
17_13	95.5	<i>Pseudocyclammina lituus</i>	Callovian-Tithonian (Kimmeridgian-Tithonian because of underlying sample)
17_12	89	<i>Cladocoropsis mirabilis</i>	Callovian-Tithonian (Kimmeridgian-Tithonian because of underlying sample)
17_11	84	<i>Pseudocyclammina lituus</i>	Kimmeridgian - Tithonian (because of underlying sample)
17_10	80	<i>Batcinella</i> sp., <i>Actinoporella podolica</i> , <i>Andersenolina alpina</i>	Callovian-Tithonian (Kimmeridgian-Tithonian because of underlying sample)
17_08	74	<i>Cladocoropsis mirabilis</i>	Callovian-Tithonian (Kimmeridgian-Tithonian because of underlying sample)
17_07	68	<i>Actinoporella podolica</i> , <i>Cladocoropsis mirabilis</i>	Callovian-Tithonian (Kimmeridgian-Tithonian because of underlying sample)
17_06	66	<i>Pseudocyclammina lituus</i>	Callovian-Tithonian (Kimmeridgian-Tithonian because of underlying sample)
17_04	49.5	Dasyclad algae <i>Actinoporella podolica</i> , <i>Triploporella</i> spp., <i>Paleodasyclads</i> sp., miliolid spp., <i>Nautiloculina oolithica</i> , <i>Pseudocyclammina lituus</i> , <i>Everticyclammina</i> sp., <i>Pseudocyclammina bukowiensis</i>	Kimmeridgian
17_03	47	Dasyclad algae <i>Triploporella</i> spp., miliolid spp., <i>Nautiloculina oolithica</i> , <i>Pseudocyclammina lituus</i>	Kimmeridgian (because of overlying samples)
17_02	38	Dasyclad algae <i>Triploporella</i> spp., miliolid spp., gastropod spp., <i>Buccicrenata primitiva</i>	Kimmeridgian
17_01	36	Dasyclad algae <i>Triploporella</i> spp., gastropod spp., <i>Buccicrenata primitiva</i>	Kimmeridgian

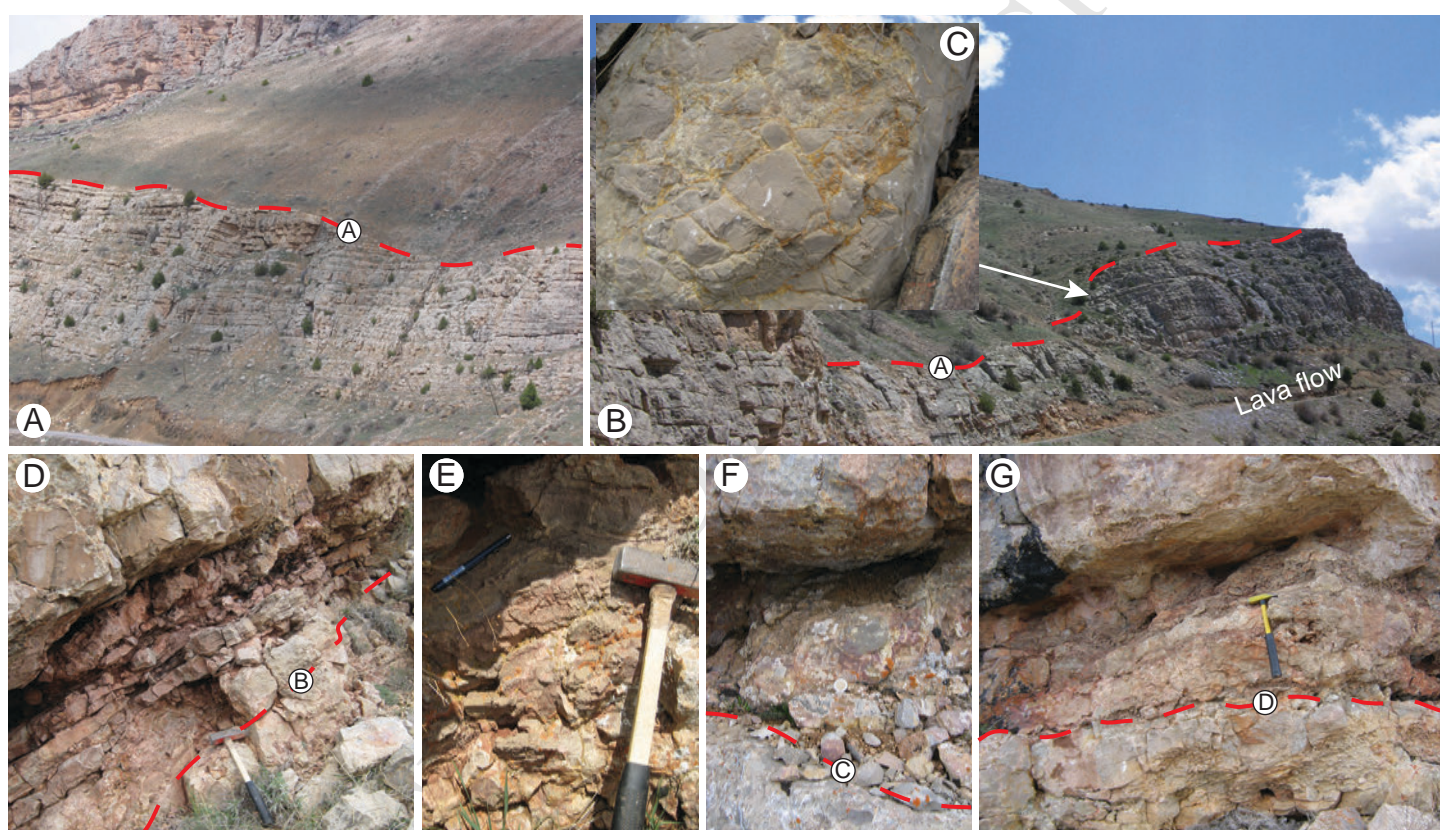


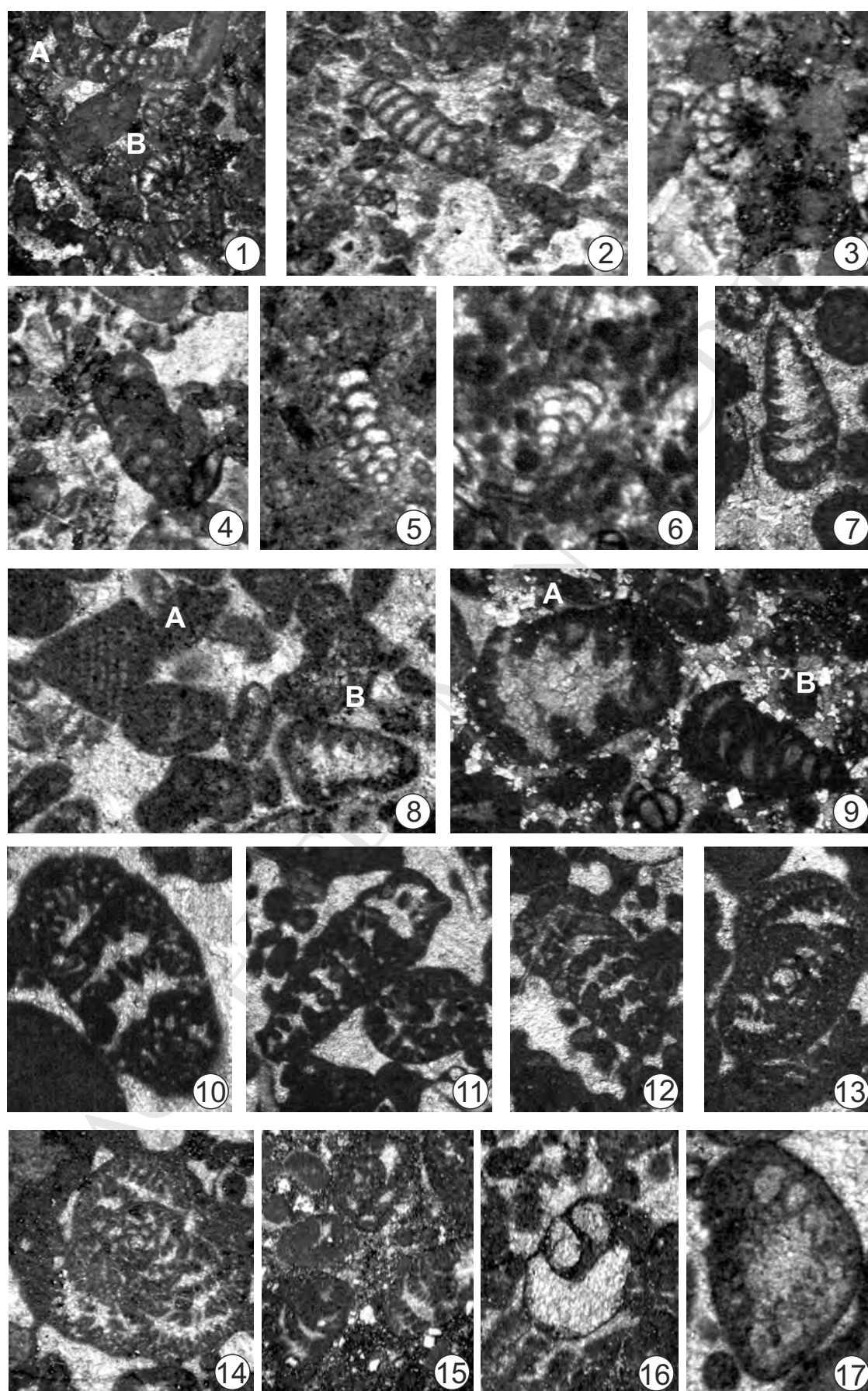


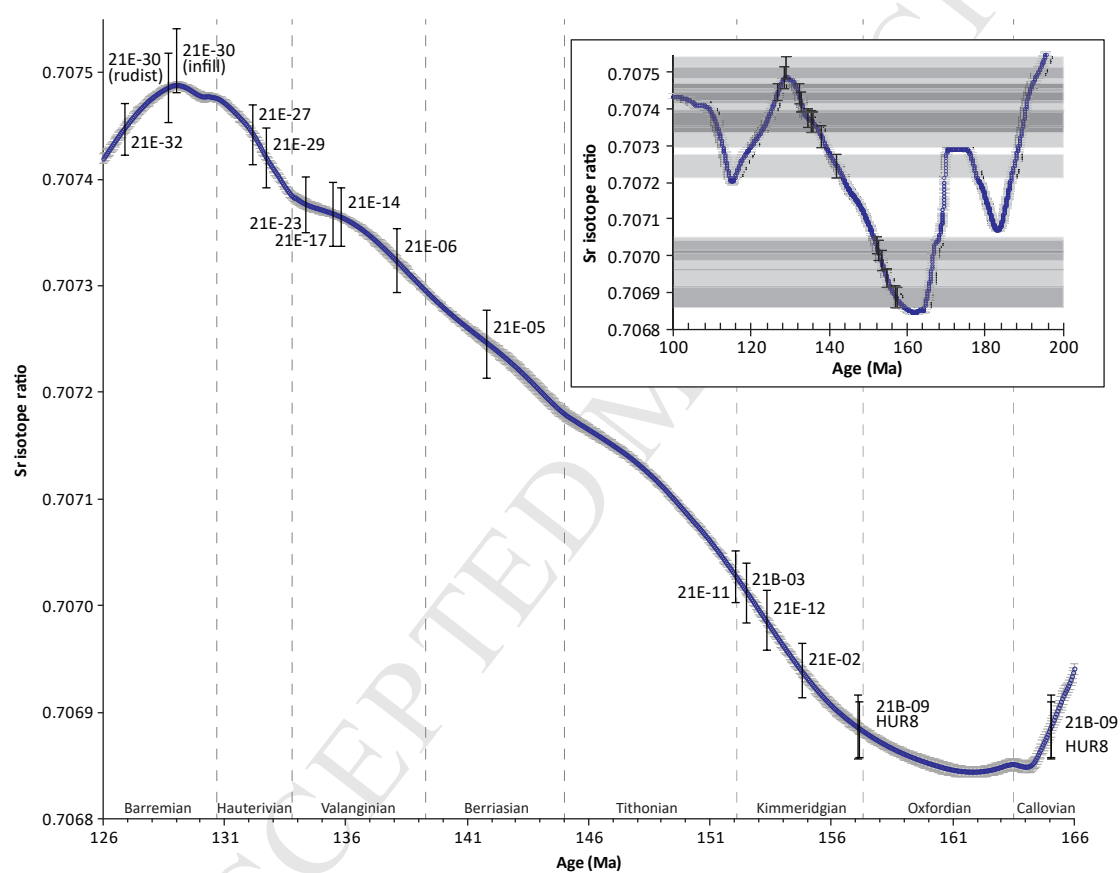


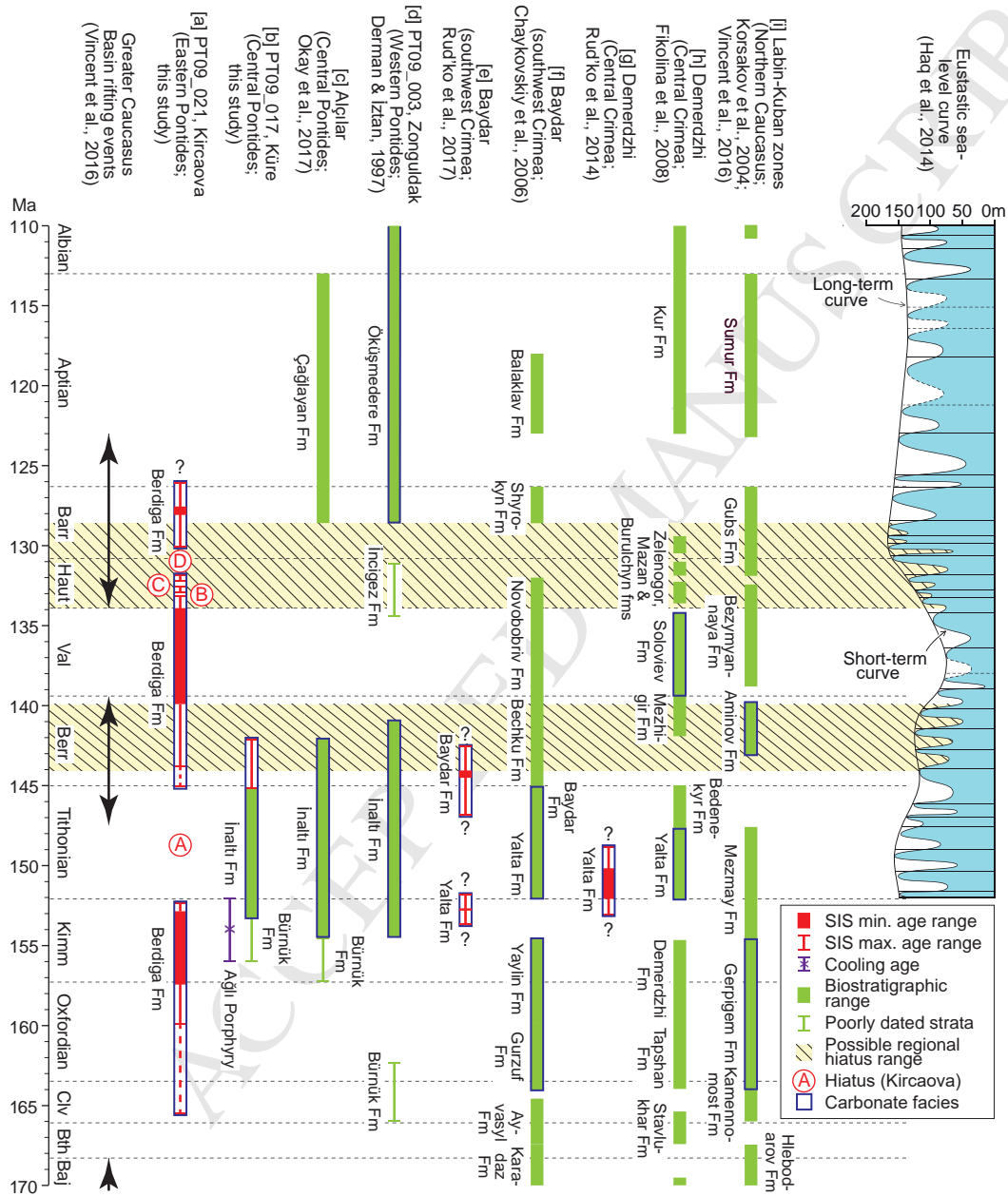


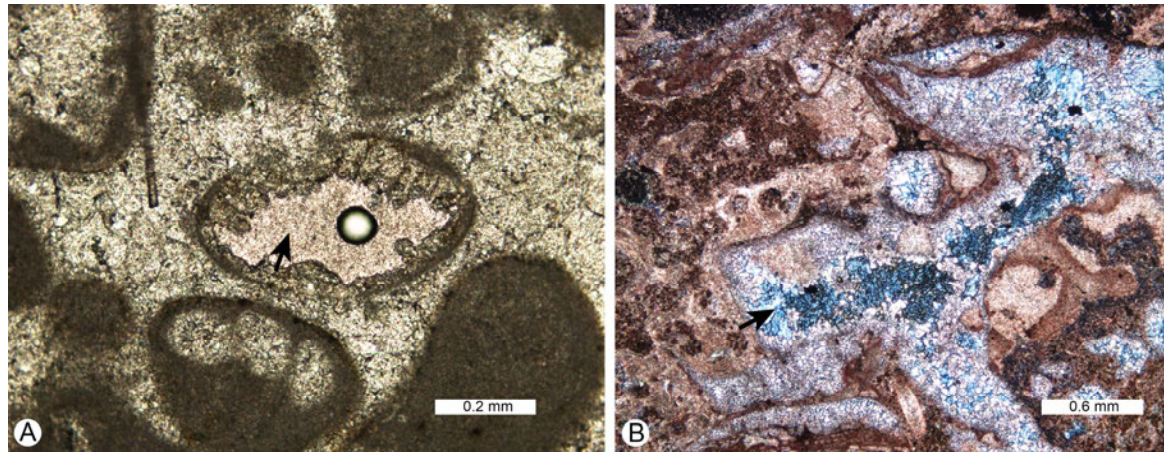












- Carbonates in the Eastern Pontides are dated using strontium isotope stratigraphy
- The age of a number of hiatuses associated with karstification are also constrained
- These span the latest Kimmeridgian to Berriasian and the Hauterivian to Barremian
- Karstification was likely caused by rift flank uplift during regional extension
- Secondary porosity development is predicted in equivalent strata in the Black Sea